Instrumentation

Infrastructure Improvements

SMARTS—Providing New Capabilities in Materials Research

M.A.M. Bourke (MST Division), D.C. Dunand (Northwestern University), E. Üstündag (California Institute of Technology)

Residual stress in fabricated components can significantly augment or detract from their service lifetimes. Accordingly, measurement of its presence helps determine whether its effect will be beneficial or detrimental. Therein lies part of the motivation behind the construction of SMARTS. This third-generation neutron diffractometer, which entered commissioning in June 2001, will provide an exciting range of capabilities for studying polycrystalline materials. Its focus includes measurement of spatially resolved strain-fields, phase deformation and load transfer in composites, the evolution of stress during temperature (or pressure) fabrication, and the development of strain during reactions (such as reduction, oxidation, or other phase transformations). The technique that underpins the instrument is neutron diffraction, which has been used to study engineering structural materials since the early 1980s.

Expanding Neutron-Diffraction Studies with SMARTS

SMARTS will expand the use of neutron diffraction to a wider range of engineering problems than is currently possible. With its extensive array of *in situ* capabilities for sample environments, it will enable measurements on small (1 mm^3) or large (1 m^3) samples. Ease of access to the sample position is one significant new feature. Components with dimensions up to 1 m and up to 1500 kg can be positioned precisely in the beam. Permanently mounted alignment theodolites (located several meters from the specimen) will provide a simple and efficient way to position samples or equipment to within 0.01 mm. Achieving this level of precision is critical for stress-strain measurements because misalignments of more than 0.1 mm can result in significant pseudo-strain artifacts.

A furnace and load-frame suite will allow research on materials under extreme loads (40,000 lb) and at extreme temperatures (1500°C). *In situ* uni-axial loading on samples up to 1 cm in diameter at stresses of 2 GPa under vacuum or in a controlled atmosphere will be routine. These values represent a significant increase over what is currently achievable.

Research Opportunities with SMARTS

Fabricated components. Residual stress in materials is often a life-determining feature because it can contribute to the aging processes by increasing susceptibility to crack formation. Interest in fabricated components crosses institutional boundaries with relevance to industry, academia, and the defense community. SMARTS will be able to accommodate large, heavy, hazardous, and radioactive samples.

New materials. Materials that could be studied on SMARTS range from cemented carbide composites for tool bits to continuous-fiber-reinforced, titanium-matrix alloys for the aerospace industry. The unique characterization capability will allow the examination of materials developed for both mundane and esoteric purposes. One particular focus will be validation of deformation models that describe microstructural effects associated with texture.

Ceramics research. One area of research that is likely to be fruitful concerns ceramics—specifically, in the study of spatial and temporal progression of solid-state reactions and phase transformations. The high-temperature, mechanical-loading capability of SMARTS will allow, for the first time, investigations of high-temperature structural ceramics and composites under almost real-life conditions.

Spatial-resolution capability. Weapons components in the stockpile must be performance-ready for many years beyond their original design life. This means that previously ignored residual stresses in critical regions (like welds) may accentuate failure modes that occur during storage and lead to unexpected failure. With SMARTS' spatially resolved capabilities (down to 1 mm^3), experiments can be made on pre-cracked samples perhaps in corrosive environments to monitor crack-tip behavior.

Understanding the implications of remanufacturing. The measurement of residual stress fields is important to the remanufacturing of weapons components. If a new or different fabrication process is used, a component may experience a different residual-stress state than its predecessor. The result may be cracking or distortion of a system that was hitherto stable. SMARTS will aid researchers by measuring the strain state of remanufactured components, which is critical to their final shape and strength, their *on-the-shelf* performance, and ultimately to their performance in a weapon system.

Process monitoring. SMARTS offers *in situ* monitoring to follow in real time powder processing, sintering, welding, mechanical alloying and design, and stress-relief procedures. Future inclusion of an environmental chamber will enable studies of *in situ* hydrogen embrittlement (HEM) and HEM-assisted crack growth in uranium and uranium-niobium alloys.

What Distinguishes SMARTS from the Neutron Powder Diffractometer?

The SMARTS mode of operation is similar to that of the current spectrometers NPD and HIPD or of the future HIPPO diffractometer. However, because the existing engineering research program takes place on the NPD, it is the most appropriate instrument for comparison. What distinguishes SMARTS from NPD is the use of a neutron guide, a T-zero (T_0) chopper, a large accessible sample area, and a six-fold increase in detector coverage.

Neutrons pass from a chilled water moderator through a series of scrapers (in the bulk shield) to the entrance of the neutron guide in ER-1. A break in the guide at 10 m from the moderator accommodates a T_0 chopper and provides space for a future frame-definition chopper. The T_0 chopper removes fast neutrons and the gamma flash (to minimize background) while the frame-definition chopper will be required if the source repetition rate is increased to 30 Hz. After the T_0 chopper, slow thermal neutrons pass down the guide to the entrance of the cave. The guide terminates approximately 3 m from the sample (at the inner surface of the cave wall). Two aperture sets (located between the exit of the guide and the sample) permit the beam cross section to be defined continuously in shape and area between 1 and 100 mm^2.

Samples will be placed on a translator that can accommodate up to 1500 kg, move in three orthogonal directions, and rotate about a vertical axis. A wide range of ancillary equipment can be accommodated on the translator, including cryostats, furnaces, texture goniometers, high-pressure cells, and load frames (Fig. 1a). Access through the roof of the cave allows large objects to be lowered into the sample position using the 15-ton (ER-2) crane. Under extreme cases, the downstream wall can be removed without affecting the integrity of the remaining cave to allow fork-lift access to the sample position. For measurements requiring spatial resolution, one of five different radial collimators (each offering different characteristics) can be supported from the roof between the sample and the detector as needed (Fig. 1b).

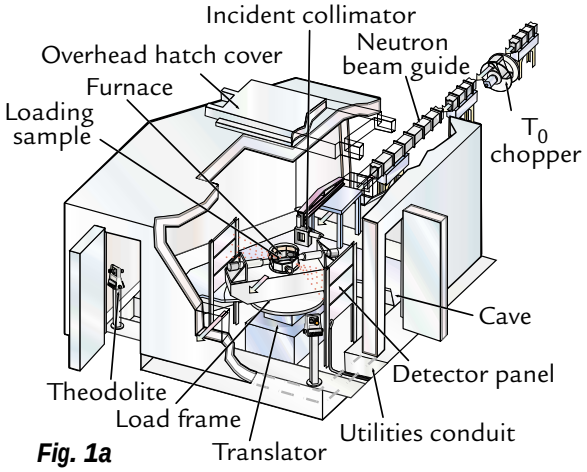

Fig. 1a

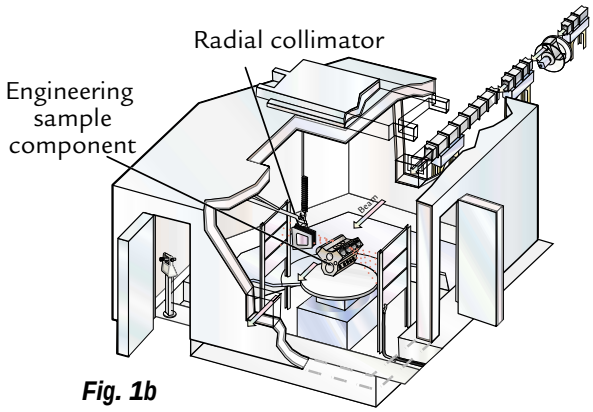

Fig. 1b

↑ **Fig. 1.** *Neutrons from the moderator pass through a series of collimating apertures before entering the neutron guide. In ER-1, a break in the guide accommodates a T_0 chopper, which removes fast neutrons and gamma flash that would otherwise contribute unwanted background. Slow thermal neutrons continue down the guide to the entrance of the SMARTS cave. On exiting the guide, neutrons pass to the center of the cave where some are scattered by the sample to the detectors. Samples or ancillary systems are placed directly on the translator, which can accommodate up to 1500 kg, move in three orthogonal directions, and rotate about a vertical axis. Theodolites provide a precise optical triangulation and alignment capability for equipment or samples. Fig. 1a (cutaway of the cave) illustrates the load-frame-furnace suite in position. Note that there is no collimation between the sample and the detector. Fig. 1b (cutaway of the cave) shows a radial collimator between the detector and a generic engineering sample. When used with the incident collimation, selection of an appropriate radial collimator defines a sampling volume for spatially resolved measurements.*

When the beam penetrates a sample, a small fraction of the neutrons interact with atoms in the material and scatter in all directions. Some are scattered to two detector banks centered on the horizontal plane at 90° to the incident beam. Each detector comprises three panels with a total of 192 ^{3}He gas-filled tubes. The panels are tilted relative to the incident beam to balance the resolution from the low to high scattering

angles. The tilt compensates for the change in resolution caused by the angular placement of each panel with a corresponding change in the sample-to-detector flight path that varies with 2θ. Interactions between the neutrons and ^{3}He in the detector tubes produce radiation that ionizes the gas, creating a cascade of electrons with associated charges. These charges are digitized and converted electronically to patterns of intensity versus scattering angle. Data from the tubes will be combined to provide TOF neutron-diffraction patterns. Analysis of the diffraction patterns will use Rietveld codes, such as the GSAS. Data acquisition will be based on VME (virtual memory extension) technology and will use Web-based visualization and control software. Experiments can be controlled remotely from the user's laboratory, and real-time data analysis will use a software package called SMARTS-EXPERT.

Residual Stresses in Manufactured Objects

When a material experiences a force (often expressed as a stress, which is force per unit area), the result is twofold. Most obvious is a distortion in shape that may or may not be visually obvious. Less obvious is a change in the amount of subsequent stress that can be applied before failure. The change can be either closer to or further from a state of failure. Any stress, no matter how small, produces these results. In the case of a stiff material (or a small stress), the change may be small, but it will always be present. What makes this significant is that the same effect can be produced in the absence of an applied stress by what is termed a residual stress.

Residual stresses are *locked into* a material in the absence of a stress. As an analogy, consider a stretched elastic band, which is then glued to a card (Fig. 2). After the glue is dry, the *stretching* force that holds the elastic band is removed. Despite the removal of this force and some limited contraction, the band remains taut because the glue holds it to the card. Accordingly, the resistance to stop the elastic band from contracting comes from the card; this resistance results in a state of residual stress between the card and the band. A qualitatively similar effect can be produced in manufactured components. (There is also stored energy in the system, which can be released if a crack propagates through the residual-stress field.)

In manufactured materials, the processing implicit in fabrication more often than not introduces residual stresses. Inhomogeneous heating and cooling, phase transformations during heat treatment, and localized plasticity during machining are all processes that can

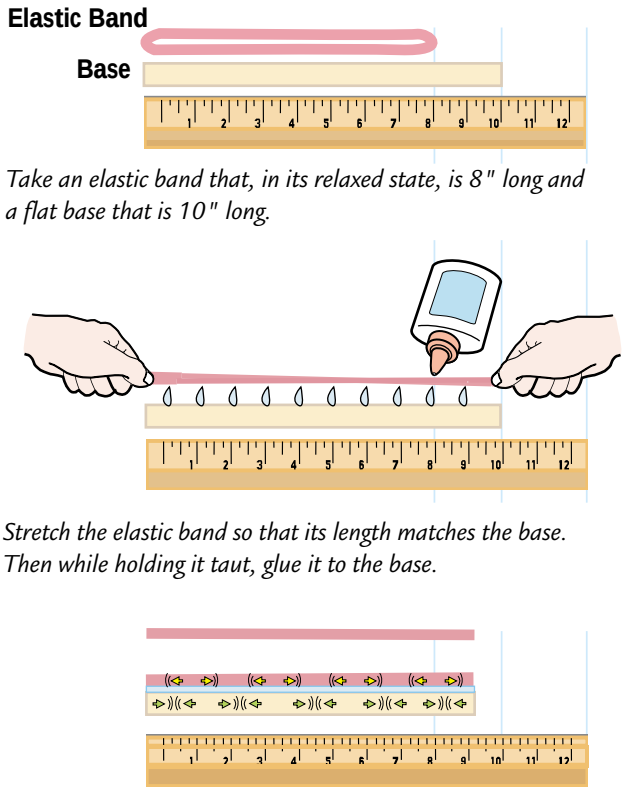

↑Fig. 2. *Residual-stress-origin analogy. Resistance to the elastic band's attempt to recover to its relaxed state come from the base, which compresses. The net effect leaves the elastic band in a state of tension (⇦ ⇨) and the base in a state of compression (⇨ ⇦). In a component, the effects that lead to residual stress are fabrication processes such as machining or welding—processes that deform one region with respect to another. The gross deformities are often invisible to the eye but may be associated with a stress that leaves the component close to failure. Also distortion may occur during subsequent operations (such as machining or heat treatment) as residual stress is redistributed.*

introduce residual stresses. In extreme cases, these processes can substantially alter the strength available for an application. Thus durability, fatigue, fracture toughness, and strength are all affected. Consequently, the ability to measure (and predict) the presence of residual stress is a critical technology for material processing, stress relief, heat treatment, lifetime prediction, and alloy design. Because a residual stress is locked inside an object, it may only become apparent long after fabrication, perhaps when a failure occurs at a significantly lower stress than anticipated resulting from a design that did not account for it (as shown in Fig. 3). In metallic objects where residual stresses may be a fraction of a millimeter or many centimeters from a free surface, a measuring tool that probes the interior is

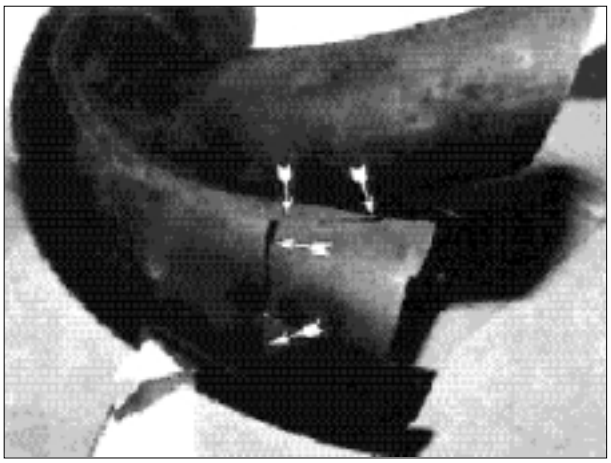

↑ ***Fig. 3.*** *Example of residual stress. This aircraft manifold cracked along a welded seam and across the dent in one of the pipes (arrows).*

needed. Neutrons penetrate many centimeters into most materials (with less attenuation than x-rays), making them ideal for examining, in a *nondestructive* manner, the interior of polycrystalline materials. The value of neutrons can be readily seen in their application to critical components, such as welds in pressurized-water-reactor vessels or in NASA rocket boosters.

SMARTS—Understanding Deformation at the Microstructural Level

In most engineering calculations, the mechanical performance of structures or components are calculated under the assumption that the material is homogeneous. Although this assumption is often sufficient, it may become dramatically invalid under atypical conditions such as heat or pressure or close to failure.

Polycrystalline materials (that comprise a large fraction of the materials used in structural engineering applications) are comprised of many individual grains (Fig. 4). These grains typically exhibit elastic and plastic characteristics that are directionally anisotropic. Elastic moduli are often anisotropic, and plasticity occurs through slip along preferentially oriented crystallographic directions. The net result is that deformation at the microstructural level is far from homogeneous!

Neutron diffraction provides a technique to study the influence of the polycrystalline structure on the strain response of individual lattice planes. Because neutron measurements can irradiate bulk volumes (as much as several cm^3), the results are statistically robust and

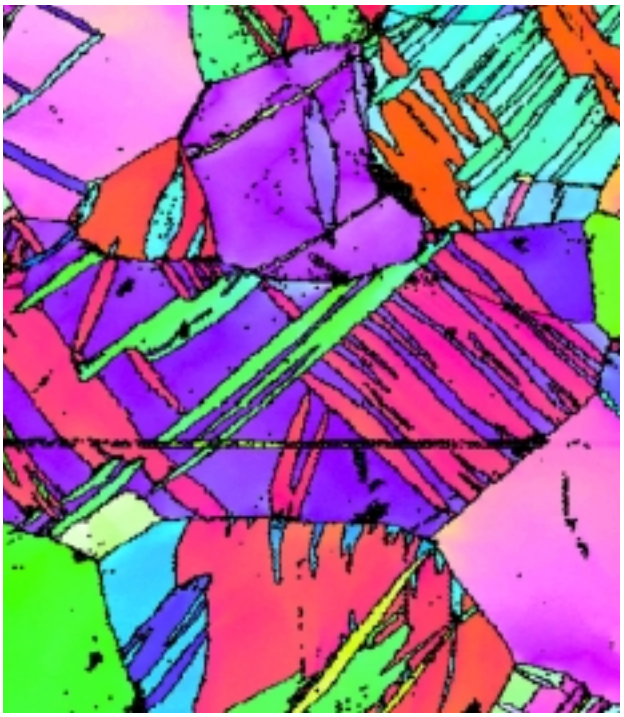

↑ ***Fig. 4.*** *False color microstructure showing grains and twins in zirconium (courtesy of George Kaschner, MST Division).*

representative of the bulk. Moreover, the ability to pass the beam through heat shields or vacuum containment simplifies performing *in situ* deformation studies under extreme conditions.

The response of different lattice planes under applied loads can be predicted with micromechanics models that either describe microstructures as discrete entities or as *average* agglomerates. For instance, self-consistent elasto-plastic polycrystalline models have predicted residual strains associated with defined texture states. The predictions were validated by *in situ* neutron diffraction measurements under load, which provided a rigorous test of the applicability and limitations of the model. However, despite some successes, models ultimately need to predict the onset and gradual evolution of intergranular strains associated with plastic cold-working. In this respect, the effects of initial texture and dislocation structure have been poorly studied, and in particular current models fare poorly when simulating large strain problems such as rolling. For this reason, neutron measurements are important because they can test the validity of modeling assumptions concerning grain reorientation (i.e., texture development) and the hardening evolution in individual grains.

HIPPO—A New High-Intensity Neutron Diffractometer for Characterizing Bulk Materials

K. Bennett, R.B. Von Dreele (LANSCE Division), H.-R. Wenk (University of California at Berkeley)

The new time-of-flight HIPPO neutron diffractometer for materials studies is under construction at the Lujan Center. The majority of HIPPO was designed and manufactured at LANSCE and is part of an upgrade project of LANSCE facilities sponsored by the DOE/OBES and DP. The development of the HIPPO instrument is a combined effort between the University of California campuses and national laboratories to attain scientific excellence in neutron diffraction, to advance our present knowledge of condensed matter, and to make neutron diffractometry an accessible and available tool to the national user community. HIPPO will allow researchers and students to conduct, for example, real-time structural studies in situ at high and low temperatures and at high pressures under a variety of environmental conditions. This unique neutron diffractometer will cover a broad variety of disciplines, including materials science and engineering, earth sciences, physics, and chemistry, and it will advance research in three interdependent material properties—high pressure, texture, and magnetism—all of which can be measured simultaneously with HIPPO. Between 150 and 250 experiments will be accommodated each year during an eight-month run cycle to benefit the neutron specialists and the materials- and earth-sciences communities. By providing easy and sustained access to HIPPO, we will open neutron diffraction to graduate-student thesis research, which often cannot wait until the formal proposal for a single experiment is approved.

Advantages of Neutron-Diffraction Applications

Important new neutron-diffraction applications have emerged in both applied and fundamental condensed-matter research. Of particular interest to the research community is the investigation of small (1 mm^3) and large (2 cm^3) sample volumes at high (< 2,000 K) and low (> 10 K) temperatures, at high pressure (< 30 GPa), and in different atmospheres. Because neutrons can travel large distances through most materials without being absorbed, they can be used to study atomic structures in bulk samples under a variety of experimental conditions. The availability of high spectral resolution also allows the simultaneous measurement of, for example, refined crystal structures, phase proportions, textures, and strains using modified Rietveld methods.[1,2]

The new HIPPO diffractometer takes advantage of the improved neutron source at LANSCE and a short flight path (flux at the sample will be nominally 10^8 $n/cm^{-2}/s^{-1}$) to overcome a major limitation of neutrons—their weak intensity. The count rate for some experiments will be approximately 20 to 60 times what is currently obtained on the high-intensity powder diffractometer presently at the Lujan Center, and researchers will be able to make measurements in as little as 5 to 10 s. It will produce, within minutes rather than hours, TOF neutron-diffraction patterns from the data output of three-dimensional detector banks consisting of about 1,400 ^3He gas-filled detector tubes. HIPPO's fast data-acquisition capability and the novel arrangement of its detectors will allow researchers to study time-dependent processes and crystal orientations in bulk samples. With the analysis of the diffraction patterns using Rietveld codes, HIPPO will fast become the instrument of choice in the fields of phase transformation, high-pressure research, polycrystal anisotropy (texture-stress-strain), and complex materials crystallography. Researchers will be able to study the dynamics of reactions, recrystallization, and deformation of bulk anisotropic properties under various temperature and pressure conditions. No existing instrument has this capability.

State-of-the-Art Technology

A state-of-the-art target-moderator system produces pulsed thermal neutrons that travel down HIPPO's initial (neutron source to sample) 9-m-long FP (Fig. 1). A T_0 chopper removes the fast neutrons, or neutrons of a particular wavelength, produced at the neutron-production target, and a collimator guides the beam down the length of the FP toward the sample chamber. Scappers—plates consisting of multiple holes varying in size from large to small (from about 8 in. down to 2 in. in diameter)—gradually reduce the size of the beam as it travels toward the sample chamber and make it more coherent and focused. As the beam penetrates the bulk material in the sample chamber, neutrons interact with the atoms that make up the material and diffract off into the three-dimensional rings of detector banks, which are set at very specific angles. An array of about 1,400 ^3He detector tubes cover nearly a 4.6 m^2 area with five detector banks at scattering angles ranging from backscattering at nominally 150° to forward scattering at nominally 10°. The detector panels are

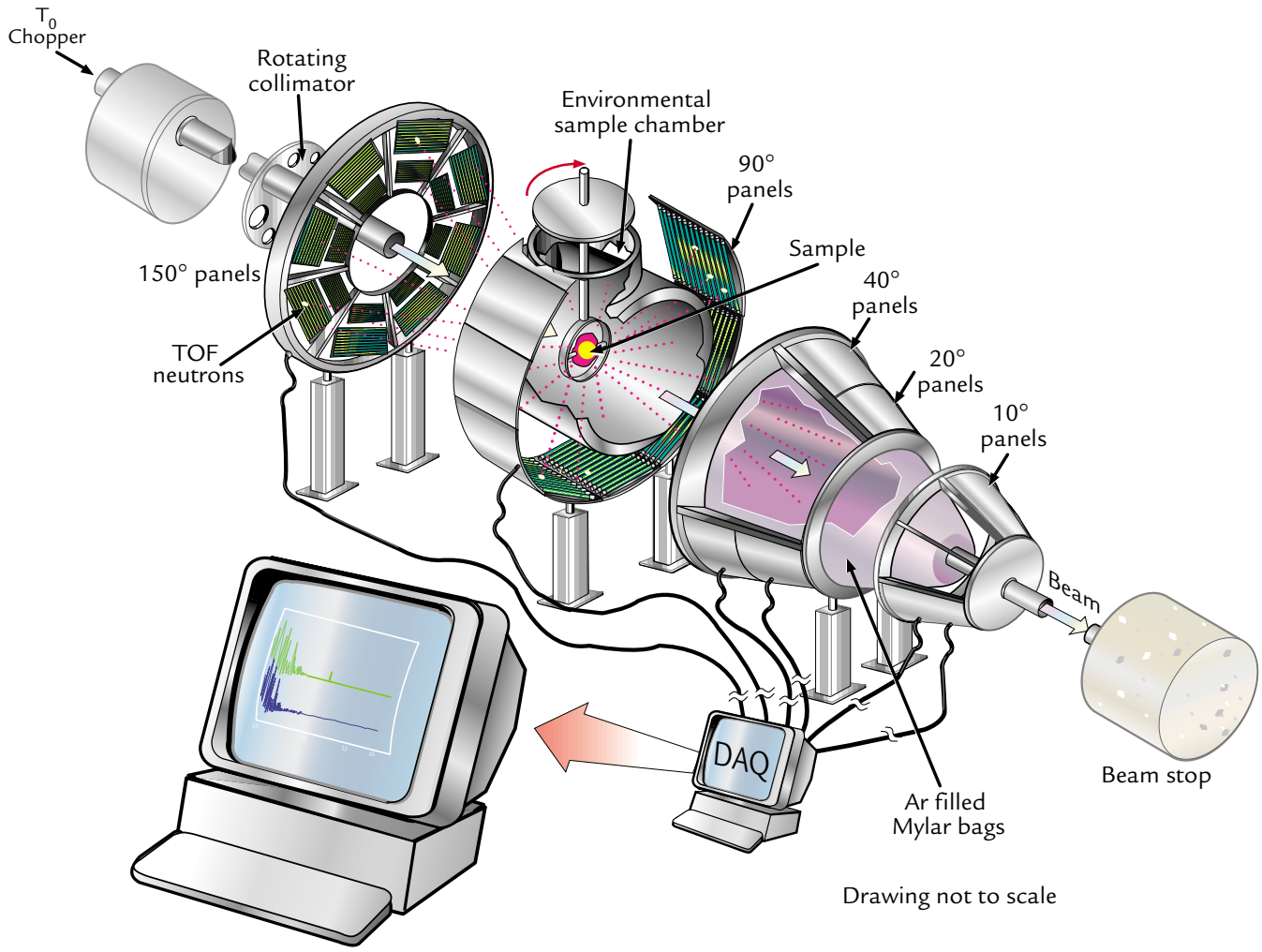

↑ ***Fig. 1.*** *Exploded view of HIPPO showing sample chamber surrounded by five conical three-dimensional rings of ^{3}He detector tubes in 10 atm. A white beam made up of pulsed neutrons of different energies (entering from the left) travels down a collimator to a chopper that cuts out very fast neutrons, allowing only slower thermal neutrons to continue down the FP to the bulk material contained inside a 29.13-in.-diam sample chamber. The neutrons interact with the lattice (crystal) structure of the bulk material, diffract off, and impinge on the detectors. We measure the neutron diffraction (in the form of light signals) to ascertain how the energies or momentum of the neutrons changed after interacting with the atoms in the lattice structure and to simultaneously determine the structure of the material.*

tilted relative to the diffracted neutron paths to give a more constant resolution across their surfaces. The tilt compensates for the change in resolution caused by the angular placement of each panel with a corresponding change in the sample-to-detector FP. The interaction between the neutrons and ^{3}He in the detector tubes produces radiation that ionizes the gas, creating a cascade of electrons with associated charges. These charges are digitized and converted electronically to data and patterns of intensity versus scattering angle.

HIPPO's extremely high count rate makes it ideal for studying time-dependent processes and small and large samples of material under a wide variety of environmental conditions. Its three-dimensional arrangement of detectors will allow researchers to make direct measurements of the orientation of crystals in polycrystalline samples either without rotating the sample or using only very few sample rotations. An innovative "sample changer" will hold 110 samples at a time for rapid powder-diffraction measurements and 64 samples at a time for rapid texture measurements (Fig. 2). A complete measurement of the crystal orientation distribution in a typical texture experiment of, for example, a 1-cm stainless steel cube will take only about five minutes to make. This measurement time will vary depending on the size, weight, and composition of the sample.

↑ ***Fig. 2.*** *Kristin Bennett, HIPPO project manager, loads a texture sample on the goniometer in the multi-position sample changer for diffraction measurements.*

A number of environmental stages, including a cryostat, furnace, a three-axis texture goniometer with Kappa geometry, high-pressure cells, and sample changer, can be accommodated within HIPPO. Data acquisition will be based on current VME technology and will make use of Web-based visualization and control software. Experiments can be controlled remotely from the user's laboratory.

Myriad Research Applications with HIPPO

We designed HIPPO to accommodate various research efforts in obtaining *in situ* neutron-diffraction data. HIPPO can be applied to research in kinetics of reactions, high-pressure investigations of complex systems with large sample volumes, the evolution of texture in polycrystals during deformation processes, and recrystallization and phase transformation studies. TOF neutron-diffraction techniques offer some unique advantages over other methods in characterizing texture. Diffraction signals average over large volumes rather than surfaces, making grain statistics for texture analysis easily obtainable. Also, because intensity corrections are generally unnecessary with this method, a high level of accuracy can be obtained.[3] The low-absorption property of neutrons allows researchers to use environmental stages (high temperature, low temperature, and bulk stress-strain) to observe *in situ* texture changes.[4,5] For pulsed polychromatic neutrons, a whole range of wavelengths is available, and continuous spectra can be recorded at moderate resolution. These types of neutrons are especially adaptive to problems of low crystal symmetry and composites with many diffraction peaks typical for modern materials and for many environmental problems.[6] The texture of such materials cannot be satisfactorily characterized by x-ray diffraction. New crystallographic methods are being used to analyze these spectra and obtain simultaneous information on crystal structure, orientation distribution, and phase proportions (from intensities), internal elastic strains (from peak locations), and microstructure (from peak shapes).[1, 2, 7] Areas of research might include texture and anisotropy studies of rocks, for example, granite-mylonite and mantle peridotites; crystal-structure studies of zeolites; and structure studies of liquids and melts, including aluminum-silicon melts and glasses.

In situ high pressure-temperature (P-T) neutron-diffraction experiments provide a unique opportunity to study texture, hydrogen bonding, magnetic moments, and structural and thermal parameters of light elements (for example, hydrogen, lithium, and carbon) and heavy elements (for example, tantalum, uranium, and plutonium), which are virtually impossible to determine by x-ray diffraction techniques. For example, we can derive thermoelasticities and Debye-Waller factors as functions of pressure and temperature using *in situ* high P-T neutron-diffraction techniques. These applications can also be extended to a much broader spectrum of scientific problems. For instance, puzzles in Earth science, such as the carbon cycle and the role of hydrous minerals for water exchange between lithosphere and biosphere, can be directly addressed. Moreover, by introducing *in situ* shear strain, texture accompanied with phase transitions in the deep mantle can also be studied by high P-T neutron-diffraction experiments. With the new HIPPO toroidal anvil press (TAP-98) designed by Yusheng Zhao (LANSCE-12),[8] we will be able to accommodate *in situ* P-T neutron-diffraction experiments up to 30 GPa and 2000 K simultaneously. Sample sizes may range from 50 to 300 mm^3. The TAP-98 is positioned in the HIPPO sample chamber at different diffraction settings. A vertical setting will serve the purpose of studying texture development under high-pressure and high-temperature conditions. The TAP-98 will also provide a transmitting port for small-angle neutron-diffraction experiments.

Neutron scattering is the prime tool when it comes to determining spatial and temporal distributions of magnetization at the microscopic scale.[9] Magnetic scattering is due to a dipole interaction between the magnetic moments of the neutron and the unpaired outer-shell electrons, and it gives rise to additional contributions in the diffraction pattern. Therefore, neutrons offer the unique capability to measure spin, charge, and lattice

effects simultaneously. Studies of magnetic scattering are effectively restricted to d-spacings greater than about 1 to 2 Å, and the HIPPO diffractometer covers significantly larger d-spacings. In addition, the large neutron flux of HIPPO will allow relatively fast measurements of magnetic materials, which often suffer from the fact that the magnetic intensities are weak compared to the nuclear ones. Finally, the HIPPO diffractometer provides novel capabilities, for example, the study of magnetic systems under pressure.

References

1. R.B. Von Dreele, "Quantitative Texture Analysis by Rietveld Refinement," *Journal of Applied Crystallography* **30**, 577-587 (1997).
2. L. Lutterotti, S. Matthies, H.-R. Wenk, A.J. Schultz, and J.W. Richardson, "Combined Texture and Structure Analysis of Deformed Limestone from Time-of-Flight Neutron Diffraction Spectra," *Journal of Applied Physics* **81**, 594-600 (1997).
3. H.-R. Wenk, "Standard Project for Pole Figure Determination by Neutron Diffraction," *Journal of Applied Crystallography* **24**, 920-927 (1991).
4. K. Bennett, H.-R. Wenk, W.B. Durham, and C.S. Choi, "Texture Analysis of High-Pressure Low-Temperature Ice Polycrystals: A Study by Neutron Diffraction," in *Textures in Geological Materials*, H.J. Bunge, S. Siegesmund, W. Skrotzki and K. Weber (Eds.), Deutsche Gesellschaft Metallkunde, Oberursel, Germany, 251-160 (1994).
5. K. Bennett, H.-R. Wenk, W.B. Durham, L.A. Stern, and S.H. Kirby, "Preferred Crystallographic Orientation in the Ice I-II Transformation and the Flow of Ice II," *Philosophical Magazine A* **76**, 413-435 (1997).
6. H.-R. Wenk, "Texture Analysis with Time-of-Flight Neutrons," in *Time-of-Flight Diffraction at Pulsed Neutron Sources*, J.D. Jorgensen and A.J. Schultz. (Eds.), *Transactions of the American Crystallographic Association*, 95-108 (1993).
7. H.-R. Wenk, S. Matthies, and L. Lutterotti, "Texture Analysis from Diffraction Spectra," in *Proceedings of the ICOTOM 10, Materials Science Forum* **157-162**, 473-479 (1994).
8. Y. Zhao, R.B. Von Dreele, and J.G. Morgan, "A High P-T Cell Assembly for Neutron Diffraction Up to 10 GPa and 1500 K," *High Pressure Research* **16**, 161-177 (1999).
9. G.E. Bacon and R.S. Pease, "A Neutron Diffraction Study of Potassium Dihydrogen Phosphate by Fourier Analysis," in *Proceedings of Royal Chemistry Society* **A220**, 397-421 (1953).

Protein Crystallography Station—Solving Protein Structures with Innovative Time-of-Flight Neutron Diffraction Techniques

P.A. Langan, B.P. Schoenborn (B Division)

Emerging efforts to solve the three-dimensional structures of thousands of proteins sequenced in genome projects are largely based on the use of synchrotron x-rays. However, certain unique types of information relating to structurally and functionally important hydrogen atoms and water molecules can only be obtained through experimentation with neutrons. Hydrogen atoms comprise roughly half the atoms of biological molecules such as proteins, DNA, and carbohydrates, and hydrogen ions are the primary motive force in many fundamental biological processes. Most biological processes take place in an aqueous environment where interaction with water is crucial. Neutron studies in general provide information that cannot be obtained by other methods and are strongly complementary to x-ray, electron microscopy, and nuclear-magnetic-resonance investigations.

The new neutron PCS located at LANSCE incorporates a number of technological innovations that, with the improved LANSCE neutron source and a large electronic neutron detector, will allow the structural biology community to collect TOF wavelength-resolved Laue data from small protein crystals and partially disordered systems, including fibers and membranes. The DOE/OBER funds the PCS, which is earmarked for commissioning in 2001. This innovative station was built by B Division with support from LANSCE and is the only resource of its kind in North America. Accommodating fifteen to twenty experiments each year during an eight-month run cycle, this station has the potential to augment the role of a variety of high throughput structural genomics programs with information about the mechanisms of newly discovered enzymes.

Protein Crystallography Station: An Overview

The PCS is located on FP15, viewing a moderator specifically tailored for protein crystallography where neutrons are emitted in pulses at a rate of 20 to 30 Hz.[1] A schematic representation of the beam layout is shown in Fig. 1. From the moderator, the neutrons travel 28 m down vacuum pipes with collimation inserts that taper the neutrons to produce a fine, almost parallel, beam that hits the crystal sample. The collimation elements extend back into the bulk shielding that surrounds the moderator where a 2-m section of beam pipe can be filled with mercury to act as a shutter for opening and closing the neutron beam.

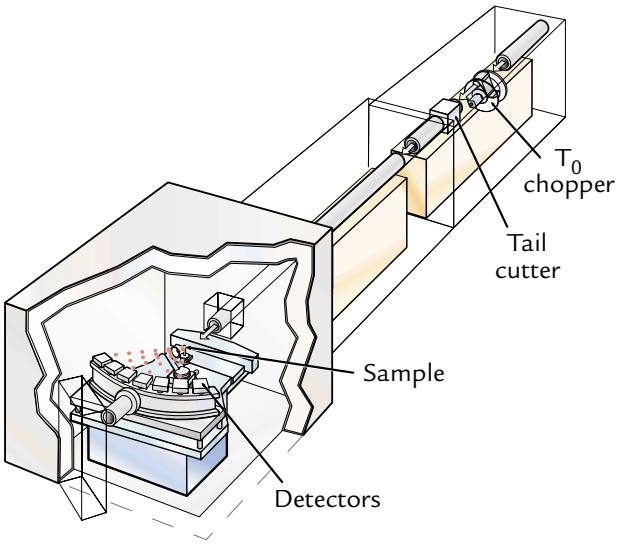

↑ ***Fig. 1.*** *PCS beam layout (courtesy of Kathy Lovell and Garth Tietjen).*

At 11 m from the moderator, the vacuum pipe carries the neutrons out of the small experimental room (ER-1) that surrounds the bulk shield and through a wall into a larger experimental hall (ER-2). The vacuum pipe is interrupted in ER-1 by two beam-shaping devices at 9.5 m from the moderator—a composite T_0/T_1 chopper and a proposed tail-cutting device. These devices remove unwanted high- and low-energy neutrons and neutrons that trail too far behind similar energy neutrons in each pulse, thus optimizing the neutron beam for high counting rates and low backgrounds at reasonable instrument resolutions. The vacuum pipe is tightly surrounded by heavy shielding until it reaches the sample position where the shield opens up to a large cave in ER-2.

In the cave, neutrons interact with atoms in the crystal sample and are scattered out of the beam in many directions. Neutrons with a wavelength that matches the spacing between a set of periodic planes of atoms are diffracted in a specific direction and produce a spot when recorded by a neutron area detector. Different planes of atoms produce a pattern of diffraction spots—a Laue pattern—that correspond to different wavelengths. A Laue pattern is recorded while a κ-circle goniometer moves the crystal and detector between about 30 different orientations. This feature enables all planes in the crystal to be brought into an orientation that will produce diffraction spots. A complete data set can consist of many thousands of diffraction spots. An optional 8-T magnet can be

mounted on the goniometer to magnetically orient membrane and fiber samples. A large cylindrical detector collects as many spots as possible at each crystal orientation without having to reposition the detector.

The positions of detected neutrons are passed from the detector to a VXI-based data-acquisition system where they are stored in memory along with their time of arrival. After a sufficient number of neutrons have been collected at a particular crystal and detector setting, the data and the parameters that describe the instrument setting are written to a data archive in the form of a NeXus file. A commercial software package called d*TREK has been customized to control data collection, display, and processing and ultimately to produce a measured intensity and an index for each diffraction spot. The index is a crystallographic description of the diffracting planes that produced the diffraction spots. The intensities and indices provide the input required by conventional Fourier-based protein-structure-refinement software that ultimately produces an image of the protein crystal's structure.

Toward Technological Innovations in Protein Crystallography

The development of neutron protein crystallography has mainly been aimed at developing strategies that overcome limitations in neutron flux by maximizing the quantity and quality of data. The effort to build a PCS at LANSCE with greatly reduced sample-size requirements has involved a number of new technological innovations. Some of these innovations described below are expected to have general applications outside of structural biology.

A Partially Coupled Water Moderator. High-energy neutrons produced by the target are slowed down to thermal or cold energies by ambient water (~ 300 K) or liquid hydrogen (~ 20 K) moderators that have been neutronically isolated (decoupled) from their surrounding. Decoupling maintains a small neutron pulse width after moderation so that very high energy and diffraction resolutions can be accessed. However, the most useful neutron pulses for structural biology have energies between 3 to 80 meV and do not require short time widths. By partially coupling a water moderator to its surroundings, the neutron flux in the intermediate "cool" energy range (~ 100 K) has been increased at the expense of resolution (Fig. 2).[2] The exact coupling has been optimized along with the instrument FP length (28 m) so that length scales down to 1.5 Å are still resolved.

Composite T_0/T_1 Chopper. The beam is tailored to a wavelength range of 1 Å to 5 Å by a novel composite rotating-blade T_0/T_1 chopper that is located at 9.5 m from the moderator. The T_0 component reduces the amount of background and protects biological samples from damage by removing fast neutrons and gamma

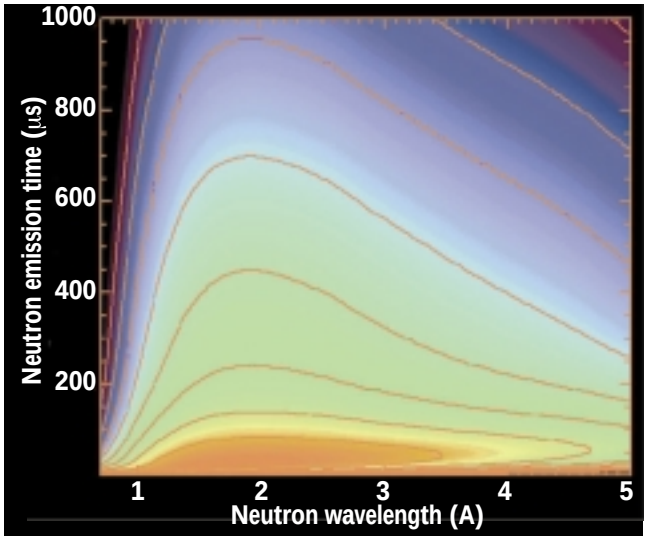

↑ ***Fig. 2.*** *Neutron emission time-wavelength probability distribution as calculated by a Monte Carlo neutron and photon transport code for the PCS water moderator located on FP15. The contours are equally spaced on a logarithmic scale. The long-time exponential decay of the pulse becomes clearly visible as the contours become equally spaced (courtesy of Luke Daemen).*

rays from the beam. The T_1 component removes frame overlap—low-energy neutrons that fall behind one pulse (trailing neutrons) and then interfere with the high-energy neutrons from a subsequent pulse. The T_0 component is a rotating nickel alloy blade (Fig. 3a) with a cross section similar to the size of the neutron beam, a length in the beam of around 12 cm, and a radius of 30 cm. The blade rotates at the same frequency as the neutron source and is in a position to block fast neutrons and gamma rays each time that a pulse of protons hits the spallation target. An aerodynamic shroud (opaque in Fig. 3a) coupled to the blade increases the lifetime of the bearings by allowing the chopper housing (red in Fig. 3b) to be filled with helium rather than a vacuum. A neutron-absorbing paint on one end of the shroud makes a T_1 blade with a window large enough to transmit 1-Å to 5-Å neutrons. T_0 and T_1 choppers are usually installed on separate motors; however, a composite chopper greatly reduces cost and maintenance.

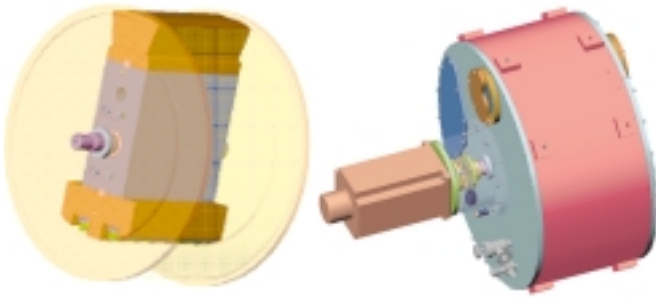

↑ ***Fig. 3.*** *(a) The chopper blade and aerodynamic shroud, and (b) the chopper housing, as described in the text (courtesy of Gerry Haas, Joe O'Toole, and Mark Taylor).*

Tail-Cutting Device for High Resolution. Most protein crystals diffract to resolutions that correspond to length scales of ~ 2 Å. In its standard configuration, the PCS can access length scales down to ~ 1.5 Å. However, for situations where unusually high diffraction resolution is required (< 1.5 Å) or when trailing neutrons cause diffraction spots to overlap, a novel tail-cutting device has been designed.[3] A nested aperiodic multilayer stack moves over an angular range of about 1.5° at the same frequency as the beam. This stack diffracts unwanted trailing neutrons in the long time tail of the neutron pulse out of the transmitted beam (Fig. 4). This device is a relatively cheap alternative to a Fermi chopper and has the advantage that it is easy to maintain.

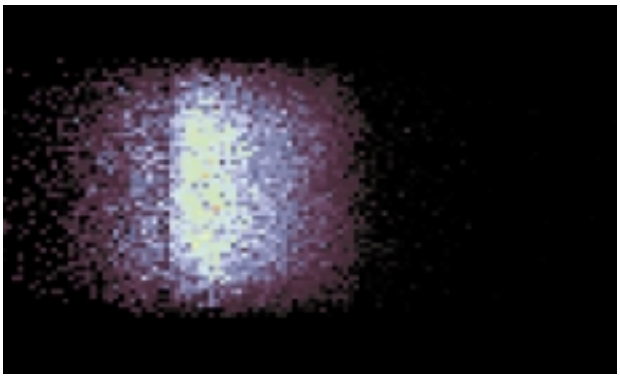

↑ ***Fig. 4.*** *Beam spot of 2-Å neutrons Bragg-reflected by the tail-cutting device out of the main transmitted beam. The "useful" transmitted neutron beam spot is centered on x = 0, y = 0, which is the beam spot at a distance of 5 m from the tail-cutting device. At a distance of 10 m from the tail-cutting device, the tail neutrons are sufficiently (spatially) separated from the early neutrons so that they can easily be removed with a small beam stop.*

A Cylindrical Neutron Detector. In addition to maximizing the number of useful neutrons that hit the crystal sample, data-collection efficiency can be greatly increased by maximizing the number of diffracted neutrons that are collected by the detector. The PCS incorporates an advanced-design gas, multiwire, proportional detector chamber. The detector, built by the Instrument Division of BNL (Fig. 5), has a height of 20 cm and a curved horizontal dimension that subtends 120° at the sample position. The detector's 70-cm radius takes into consideration the peak-to-background ratio, spot overlap, the detector spatial resolution, and engineering considerations. Parallax and window thickness limits the height of the detector. Although neutron-image-plate detectors and scintillation detectors are cheaper, can be made larger, and have higher absolute counting rates, they have other features that limit their usefulness for TOF protein crystallography.

The PCS detector has a novel electrode arrangement and signal-processing system that gives a contiguous

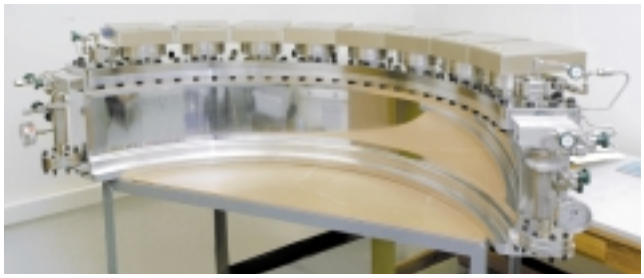

↑ ***Fig. 5.*** *The PCS cylindrical neutron detector. The detector consists of an electrode structure contained in an aluminum pressure vessel. The pressure vessel is filled with a mixture of ^{3}He and propane. The ^{3}He has an extremely high cross section for thermal neutron absorption. Neutrons diffracted by the sample are absorbed by the ^{3}He. This interaction results in the creation of a proton and triton. These primary ionization products drift toward the nearest electrode-anode wire where they multiply in the high electric field near the wire surface. The charges induced over different electrodes allow for the spatial detection of an event.*

detecting medium of 150 cm x 20 cm with a spatial resolution of 1.2 mm and a maximum counting rate of 10^6 ns^{-1}.

Shielding. Shielding at a spallation neutron source is more difficult than at a reactor because of the presence of high-energy neutrons. As part of the Accelerator Production of Tritium project at Los Alamos, selected neutron cross sections have been extended up to 150 MeV, and Monte Carlo code has been developed to use these cross-section libraries. LANSCE has developed a technique for using Monte Carlo codes to calculate absolute neutron and gamma-ray dose rates at the surface of neutron-beam-line shields. This technique has been applied to the design of the PCS shielding.[4] A variety of laminated shields of iron/polyethylene/iron, borated wax, and magnetite concrete around different beam-line components (e.g., choppers, scrapers, experimental caves, and beam stops were considered) have been investigated with a view to maximizing the efficiency of the shielding and minimizing the material costs. The section of vacuum pipe in ER-1 is shielded by an iron and polyethylene laminate, with some of the polyethylene impregnated with boron. In ER-2, a magnetite concrete and polyethylene shield is used. The sample cave is constructed from monolithic blocks bolted together. Each block corresponds to a steel container filled with 8 in. of 5% borated polyethylene. The interior walls of the cave are also lined with 1 in. of polyethylene.

Research Applications

Hydrogen atoms participate in interactions that determine the structure and properties of biological macromolecules and materials. (Macromolecules are composed of much larger numbers of atoms than ordinary molecules. Biologically important proteins and nucleic acids are among the many substances that are made up of macromolecular units.) But determining

hydrogen positions in crystals, fibers, or membranes of biological macromolecules is often difficult. Because of their low scattering power for x-rays, hydrogen atoms are generally not seen in protein or biological polymer structures determined by x-ray crystallography except at ultra-high resolutions (< 1 Å). In the Protein Data Bank,[5] the sole international repository for macromolecular structure data, fewer than 1% of structures attain these resolutions—the majority of structures fall well below (> 2 Å). The scattering of neutrons by hydrogen or deuterium is comparable to that of other atoms with the result that neutron diffraction has been used to obtain the positions of hydrogen atoms at typical diffraction resolutions (Fig. 6). In studies of enzyme mechanisms, neutron protein crystallography has been a powerful tool for determining key details of hydrogen structure around catalytic sites. Much of our detailed understanding of serine-proteinases, aspartic proteinases, and glucosidases has come from neutron diffraction. The unique information that can be derived from neutron protein crystallography is of exceptional importance in the understanding of enzymatic mechanisms. Similarly, the protonation states of functionally important residues in the oxygen-transport protein, myoglobin, have long been of interest, and neutron diffraction has provided direct evidence of these states.

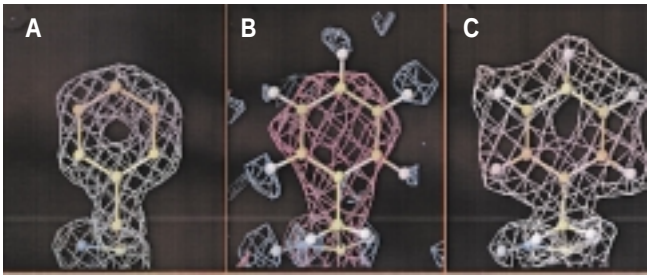

↑ ***Fig. 6.*** *Details of scattering density maps calculated from x-ray and neutron data collected from myoglobin, a protein found in muscle cells that functions as an oxygen-storage unit, providing oxygen to the working muscles. Fig. 6a shows the scattering density of myoglobin calculated from 1.8-Å x-ray data. Only carbon atoms are covered. Fig. 6b shows the negative (blue) and positive (red) scattering density of myoglobin calculated from 2-Å neutron data. Hydrogen with its strong negative scattering length is covered. Fig. 6c shows the positive scattering density calculated from 2.2-Å neutron data collected from perdeuterated myoglobin. Deuterium with its strong positive scattering length is covered. Neutron diffraction has been used to locate individual protons at catalytic sites.*

Much of the activity of biological macromolecules takes place in water. Changes in the aqueous environment can dramatically change the structure and function of biological macromolecules. At the resolution of most x-ray diffraction studies, water molecules are located with very poor reliability. Because D_2O molecules diffract neutrons strongly, ordered water molecules can be detected as easily in a neutron study as a sulfate ion in an x-ray study. Neutron diffraction studies on the vitamin B_{12} coenzyme, DNA, and other proteins and hormones have provided a wealth of unique information on the hydration of biological macromolecules.

Conclusion

Neutron diffraction has provided many important contributions to our understanding of biological structure, function, and dynamics over the past thirty years. Today the study of biological structure is going through a transformation. An explosion of three-dimensional protein structures is expected from structural genomics. The structure of complex systems consisting of assemblies of smaller proteins and nucleic acids are being studied to understand cellular processes. Biomaterials, biosensors, and food technology are becoming more important. Neutron diffraction can play an important role by providing unique types of information in this rapidly expanding field. As the only facility of its kind in North America and as a world-wide state-of-the-art instrument, the PCS will be one of the main tools for realizing this potential.

References

1. P.D. Ferguson, G.J. Russell, and E. Pitcher, "Lujan Center Cold Moderators: Current Design and Future Options," in *Proceedings of the International Workshop on Cold Moderators for Pulsed Neutron Sources* (Organization for Economic Cooperation and Development, Argonne, Illinois, 1997), 67-72.
2. B.P. Schoenborn, J.D. Court, A.C. Larson, and P.J. Ferguson, "Moderator Decoupling Options for Structural Biology at Spallation Neutron Sources," *Neutron Research* **7**, 89-106 (1999).
3. P. Langan, L. Daeman, and B.P. Schoenborn, "A Novel Optical Insertion Device for Removing the Time Tail from Spallation Neutron Pulses," submitted to Society of Photo-Optical Instrumentation Engineers Forty-Sixth Annual Meeting (San Diego, California, 2001).
4. G.J. Russell, P.D. Ferguson, E.J. Pitcher, G. Muhrer, and E. Snow, "A Methodology for Calculating Absolute Total Dose Equivalent Rates for Spallation Source Beam-Line Shielding," in *American Nuclear Society Proceedings of the Third International Topical Meeting on Nuclear Applications of Accelerator Technology* (1999), in press.
5. F.C. Bernstein, "The Protein Data Bank," *Journal of Molecular Biology* ***112,*** 535-542 (1997).

ASTERIX—A New Spectrometer for Studies of Nanomagnetism and Magnetic Properties of Complex Materials

M.R. Fitzsimmons, F. Mezei (LANSCE Division)

The development of neutron spin and sample excitation correlation techniques is essential for understanding a wide range of magnetic and electron transport problems in the emerging class of complex materials, including, for example, nanostructure-engineered and -adaptive materials. A detailed understanding of complex materials requires studies that use neutron beams to characterize the exotic magnetic and atomic structures of these materials under extreme conditions of high-magnetic fields, high pressures, and very low temperatures. Neutrons offer the unique possibility of scattering from spin and orbital moments in the material in addition to the normal scattering from atomic nuclei.

Complex instrumentation issues involved in extracting a polarized neutron beam from a pulsed neutron source and in propagating the beam through magnetic field gradients that depend upon space and time must first be understood. A solution to the polarization problems, e.g., beam splitting (the Stern-Gerlach effect), associated with interactions between (polarized) neutron beams and the equipment (in this case the high-field magnets) used to produce a variety of extreme environments simultaneously must also be developed. The solution to this problem will enable unique studies of complex materials.

Enabling the Pursuit of Scientific Frontiers in Magnetism

Traditionally, small free-standing polarizing supermirrors are used to polarize neutron beams at continuous and pulsed neutron sources. Unfortunately this approach throws away long-wavelength neutrons in favor of polarizing the short-wavelength neutrons. Why this is so can be appreciated as follows. The divergence of the neutron beam incident on the polarizing mirror is constrained (via mechanical slits) so that the neutrons reflected (or transmitted if a transmission supermirror is used) are polarized to > 95% for a particular wavelength. At a continuous source such as a reactor, the wavelength is typically ~ 4 Å with a wavelength spread of ~ 2%. At a pulsed source, that particular wavelength corresponds to the shortest wavelength of interest; however, it is also desired to polarize neutrons with wavelengths an order of magnitude longer than the shortest within the same period of the neutron pulse. Although the cold portion of the neutron beam is also polarized by the mirror, the constraining slits defining the incident beam divergence—which are required to polarize the shortest desired wavelength neutron—block many long-wavelength neutrons that would be polarized otherwise.

The goal of ASTERIX is to produce a highly polarized intense beam of cold neutrons that has a very large cross section (2 cm by 12 cm) and covers a wide wavelength range from the Lujan Center spallation target—and to do so while minimizing the fraction of the neutron beam that is not used. The project achieves its goal by embedding polarizing transmission supermirrors inside a nickel-coated neutron guide. The neutron guide replaces the constraint of mechanical slits, which produce a neutron beam of fixed divergence, with one that constrains the beam divergence to vary proportionally with wavelength. Properly arranged within the guide, the supermirrors produce a polarized neutron beam with divergence that scales with wavelength; thus, no neutrons are wasted. Crucial to the success of this project was the acquisition of high-quality polarizing transmission supermirrors.

ASTERIX will allow researchers to pursue investigations of lateral and depth non-uniformity in magnetic (or electronic) heterostructures of induced (or coerced) magnetization at or near interfaces and magnetic-structure characterization. In addition to studies of nanostructured materials, ASTERIX enables research into magnetically ordered novel bulk materials—for example, diffraction measurements of materials in very high magnetic fields using cold neutrons.

Investigating the Influence of Measurement Conditions

ASTERIX received first beam during the last 48 hours of the 2000 run cycle. This beam allowed us to determine that a cooled block of beryllium does a very good job removing undesirable high-energy neutrons and that our slits are opaque to neutrons. In addition, we demonstrated extraction of a neutron beam with modest polarization.

During the first week of the 2001 run-cycle, the red spectrum (red curve, Fig. 1) was measured for a highly collimated beam (achieved using fine slits). The

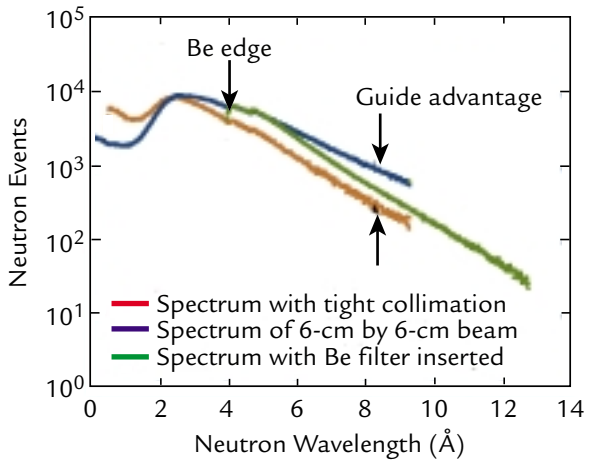

↑ Fig. 1. *Variation of spectra measured for ASTERIX under different measurement conditions, including (1) tight collimation, (2) without slits in the neutron beam, and (3) with a beryllium filter.*

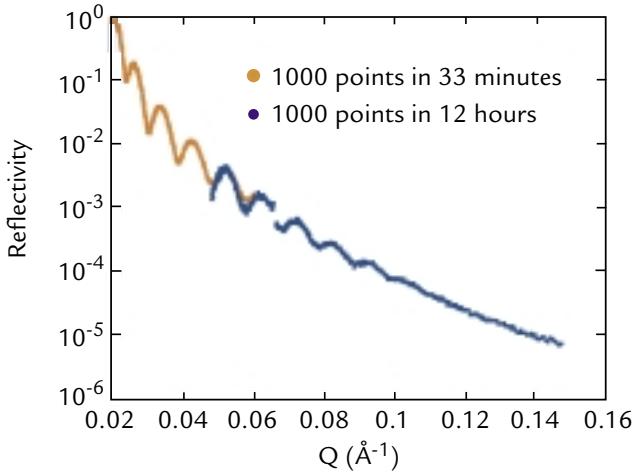

↑ Fig. 2. *Reflectivity profile of a thin nickel film grown on a 5-cm-diam silicon substrate.*

variation of the red spectrum with wavelength is exactly the same as that measured for SPEAR. Unlike SPEAR, ASTERIX views the moderator through a ^{58}Ni-coated neutron guide. As such, a slower decay in the spectrum is expected when neutrons reflecting from the guide surfaces are permitted to enter the neutron detector (or, more importantly, interact with a sample). The spectrum measured by the neutron detector without any slits in the beam (the beam cross section at the end of the guide is 6 cm by 6 cm) is shown by the blue curve. An upcoming challenge will be to develop experimental techniques to do reflectometry and diffraction measurements that relax requirements for tight collimation. Fig. 2 shows first reflectivity data taken using the new ASTERIX spectrometer. The profile was taken for two sample settings using a single ^{3}He pencil detector. The variation of the neutron spectrum (shown in Fig. 1) was removed from the measured data to obtain the profile shown in Fig. 2. No background was removed from the measured data.

The reflectivity data shown in Fig. 2 were taken from the sample positioned between the pole pieces of the electromagnet (Fig. 3). The diffractometer (courtesy BNL) consists of a World War II 5-in. gun mount from a merchant marine ship, which is now used to position the sample and orient the position-sensitive detector (whose housing is to the right of the picture, which is shown in Fig. 4). Situated behind the electromagnet in Fig. 3 is a second detector—a bank of 30 position-sensitive tubes that are used for measurements of large d-spacing Bragg reflections from single-crystal and polycrystalline materials. To the right of the electromagnet is an rf gradient-field spin flipper obtained through a

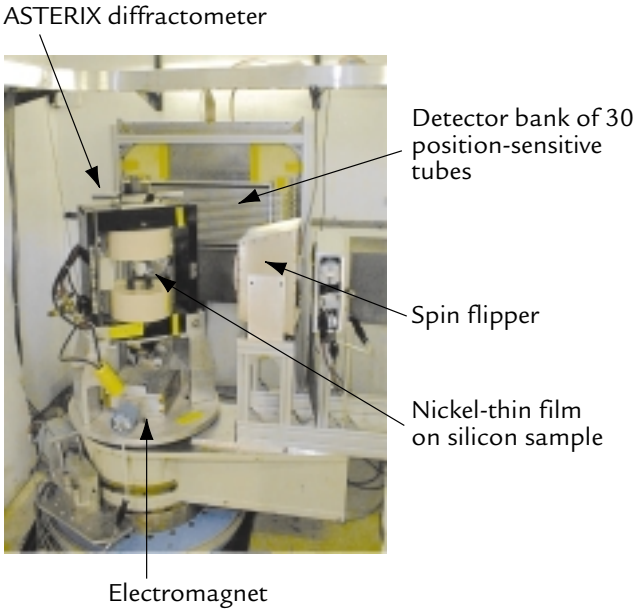

↑ Fig. 3. *View of the ASTERIX diffractometer on which a large electromagnet rests.*

collaboration with the Hahn-Meitner Institute. The neutron optical equipment used to filter (for example, the beryllium filter) and polarize (for example, the polarization-analyzer cavity) the neutron beam are out of view to the left of the diffractometer.

In Fig. 4, a pair of slits (to reduce background) are behind the spin flipper, followed by a 1-m-long polarization analyzer (a mirror inside the gray structure) and

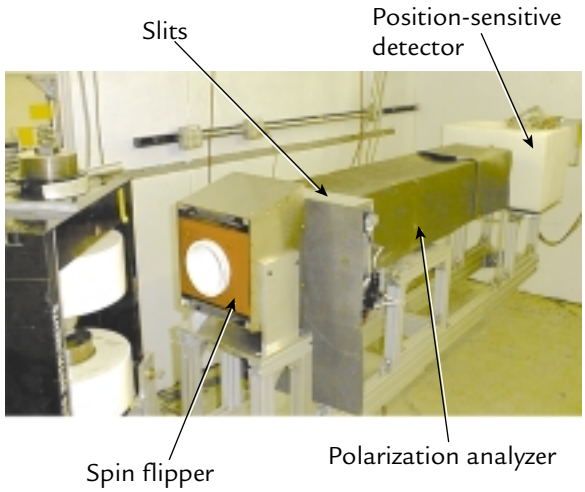

↑ ***Fig. 4.*** *View of the position-sensitive neutron detector, the polarization analyzer, the slits, and the spin flipper.*

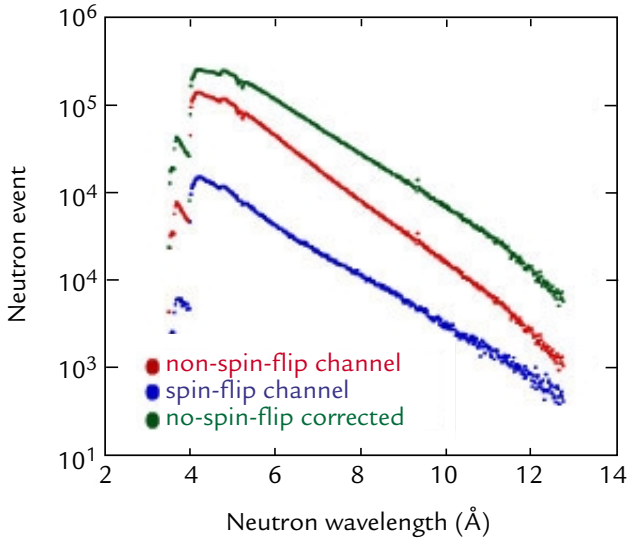

↑ ***Fig. 5.*** *Polarized neutrons are produced on ASTERIX using novel polarization-cavity technology (novel for pulsed neutron sources!).*

finally a borated polyethylene shield house for the position-sensitive detector. This detector can be moved from -10° to +30° about the axis of the diffractometer (the vertical axis passing through the electromagnet).

We measured the polarization of the neutron beam by illuminating a second neutron polarizer—the polarization analyzer—with the 2-cm-wide by 12-cm-tall neutron beam from the polarization cavity. Non-spin-flip neutrons (neutrons with spin anti-parallel to the laboratory magnetic field) are transmitted through the relatively thick silicon substrates on which the neutron-polarizing material was deposited. The intensity of the transmitted neutron beam was measured by a ^{3}He pencil detector. Spin-flip neutrons (those undesirable neutrons with spin parallel to the laboratory magnetic field) were reflected by the polarization analyzer. The intensity of the reflected neutron beam was measured by a second ^{3}He pencil detector. The ratio (called the flipping ratio) between the transmitted and reflected neutron-beam intensities (as measured by the two detectors) relates to the polarization of the neutron beam—the larger the ratio, the higher the polarization of the neutron beam.

The raw data obtained across the entire 2-cm-wide by 12-cm-tall neutron beam for non-spin-flip and spin-flip neutrons are shown as the red and blue curves, respectively, in Fig. 5. The transmitted (non-spin-flip) neutrons traveled through the thick silicon substrates of the polarization analyzer, whereas the spin-flip neutrons did not because they were reflected off the surface of the polarizer. As such, we corrected the data for the non-spin-flip channel for losses resulting from absorption (green curve, Fig. 5). We obtained a neutron-beam polarization of 95% by considering the ratio of the green curve (non-spin-flip cross section, corrected) to the blue curve (spin-flip cross section).

Although we had hoped for better polarization, 95% polarization is typical for neutron spectrometers at pulsed sources and the ADAM spectrometer at the ILL. The installation of new polarizing supermirrors from the Hahn-Meitner Institute in the polarization cavity should increase the polarization of the neutron beam to 97%.

During the first week of beam in 2001, we made an important measurement demonstrating the capability of ASTERIX to obtain diffraction patterns from small samples in the wide-angle regime in record times. Specifically, we studied a 2-mm x 2-mm x 1-mm $LaSrFeO_4$ sample. The intensity measured using just one tube in the position-sensitive detector array as a function of d-spacing is shown in Fig. 6 for two sample orientations. In the upper curve, several nuclear Bragg reflections are observed. Nearly 150,000 neutron counts were measured during a 16-h run in the (020) Bragg reflection. We compared the results obtained from ASTERIX with those taken for the same sample on the SCD. For the large d-spacing reflections [those relevant to studies of magnetism and complex (large unit cell) materials], ASTERIX out performed the SCD by more than a factor of 500. The lower curve shows the (021) Bragg reflection that is purely magnetic in origin (due to the antiferromagnetic order in $LaSrFeO_4$).

This demonstration is important in that we can show that even with the 30-T pulsed magnet operating at a

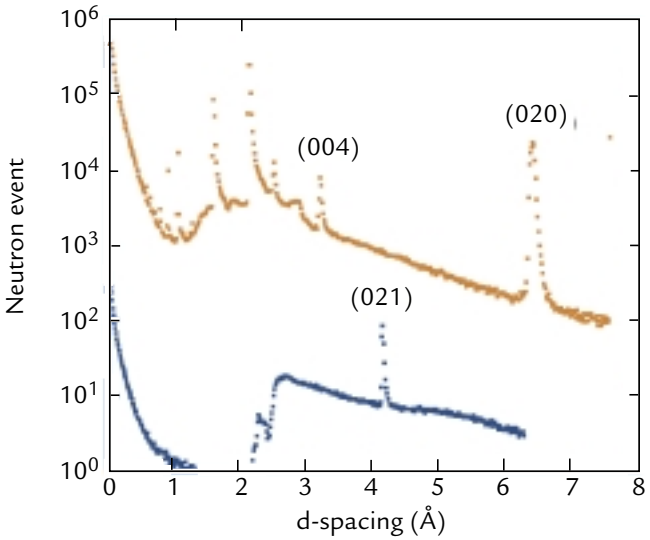

↑ ***Fig. 6.*** *Intensity measured as a function of d-spacing for two orientations of a $LaSrFeO_4$ sample.*

frequency of 1 Hz (thus only one in twenty neutron pulses provide useful information), we still have sufficient neutron flux to observe large d-spacing Bragg reflections. For example, we anticipate that typical experiments using this magnet will require roughly 12 h of beam time (equivalent to 0.4% of the magnet's lifetime). Not only will the high flux of ASTERIX be important to the pulsed-magnet program, the high flux also enables studies of very small samples—samples that might be small due to content of actinides, or due to the availability of neutron isotopes.

IN500—New Capabilities in Spectroscopy on Pulsed Sources: Adjustable Pulse Repetition Rate, Resolution, and Line Shape

M. Russina (LANSCE Division), F. Mezei (LANSCE Division and Hahn-Meitner-Institut)

Spectroscopy with cold neutrons is one of the most important areas of current superiority of reactor-based instruments over those at spallation sources. This is particularly due to the capability of continuous source TOF spectrometers to use instrumental parameters optimally adapted for the best data-collection rate in each experiment. These parameters include the pulse repetition rate and the length of the chopper pulses to achieve optimal balance between resolution and intensity. In addition, the disc chopper systems used provide perfect symmetrical line shape with no tails and low background. We present a set of novel techniques comprising the IN500 project at LANL based on the use of extended pulse length, coupled moderator, disc chopper system, and advanced neutron optical beam delivery to enable spallation sources, such as the Lujan Center, to surpass the best reactor sources in cold neutron spectroscopy by realizing the above listed key capabilities on a spallation source.

Enhanced Efficiency by Repetition Rate Multiplication

Most neutron-scattering research today is performed on steady-state reactor sources. However, the next generation of neutron sources will be pulsed. In this new situation, we face the challenge of developing novel neutron scattering techniques, which will make all instruments at pulsed sources competitive with reactor source instruments. An example of such instruments is the IN500 at LANSCE. IN500 is a cold neutron TOF spectrometer, which will offer all the advantageous capabilities of reactor-based instruments. It makes use of three innovations, each of which represents an improvement in sensitivity by a factor of three to ten compared to existing techniques. The first innovation is the use of a coupled neutron moderator, installed for the first time at LANL in the course of the current upgrade in 1998; the second innovation is the use of a reduced-loss, "ballistic" neutron guide to transmit higher neutron intensity to the sample over large distances; and the third, the use of repetition rate multiplication (RRM) to enhance the efficiency of pulsed sources in applications that can take advantage of higher pulse repetition rates than that of the source. In addition, the IN500 chopper system also will act as a pulse-shaping device to provide improved line shape for better signal-to-background ratio and to provide variable resolution capability in order to optimize the flux according to the experimental requirements.

One major source of reduced data-collection efficiency in neutron-scattering spectrometry at pulsed sources is the large difference between the repetition rate of the source and the repetition rate required by the instruments. The optimal repetition rate of TOF spectrometers is determined by the time needed to analyze the scattered neutron spectra over the flight path of 2 to 6 m in the secondary spectrometer, which is in the range of 100 to 500 Hz, whereas the repetition rate of existing and planned pulsed spallation sources is 10 to 60 Hz. The conventional principle of working with only one monochromatic wavelength per pulse only allows us 10% to 50% efficient use of the available data-collection time. The RRM principle[1] enhances efficiency by using several neutron pulses on the sample with several monochromatic lengths from each source pulse, instead of a single wavelength. The repetition rate of the instruments thus becomes independent of the source repetition rate, and it will be defined by the requirements of the experiments, similar to the spectrometers on reactor sources.

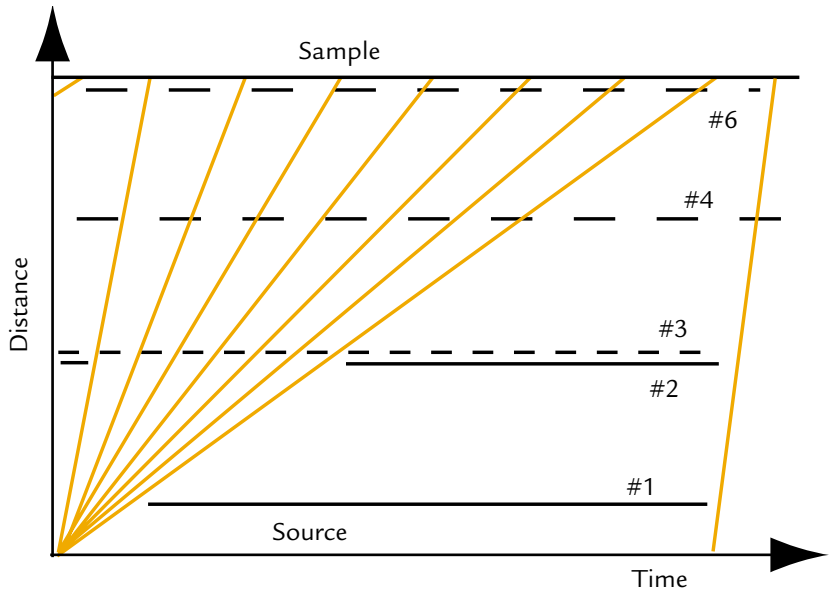

↑ ***Fig. 1.*** *Principle of RRM as realized by a disc chopper system. The source-to-sample distance in the IN500 is 63 m, and time between source pulses is 50 ms.*

In the IN500, RRM will be realized by a disc chopper system (Fig. 1), which combines features from other TOF spectrometers such as IN5 at ILL and NEAT at the Hahn-Meitner Institute (HMI) with conventional wavelength band choppers at spallation sources. The slow choppers #1 and #2 rotating with the same frequency (20 Hz) as the source define a broad wavelength band, which is later cut into a set of monochromatic pulses by fast choppers #3 and #6, also defining the primary and secondary resolution of the instrument. While slow choppers are designed to avoid overlap between neutrons coming from different source pulses, fast choppers are aimed to avoid the overlap between neutrons of different wavelengths coming from the same source pulse. In particular, chopper #4 eliminates spurious contributions coming from the long time tail of the source pulse up to 4 ms and "leaking" through the resolution-defining choppers #3 and #6. The function of chopper #5, not shown in the figure, is to suppress every second, third, or fourth pulse from the basic 240-Hz pulse rate at the sample in order to prevent the frame overlap of scattered neutrons in the secondary spectrometer between the sample and the detectors.

The IN500 chopper system was designed and optimized by the new approach of "wavelength filtering," proposed by F. Mezei, one of the authors of this article. The main principle is to divide the chopper system into independent subunits of lower numbers of choppers. First, the transmission is studied for such subunits alone, and an upper limit of the transmission of the total system is built as an overlap between the transmissions of the subunits. This overlap was then maximized by the shifting in time (phasing) of the subunits relative to each other. Fig. 2 shows the pulse sequence in time on the sample for the complete choppers system (with no pulses suppressed by chopper #5). The first (shortest wavelength) and the last (longest wavelength) pulses from subsequent source pulses overlap (double pulse in the figure) and will be eliminated in data collection. All the other pulses are cleanly separated, and all possible parasitic pulses (not shown) have wavelengths above 90 Å and therefore negligible intensities. The wavelength difference between subsequent pulses from one source pulse is 0.2646 Å, and the 2.91 Å wavelength band between the shortest and longest ones is freely chosen between 2 and 20 Å.

Adjustable Resolution

The pulse shape at spallation sources has a strongly asymmetric form resulting in an asymmetric form resolution function of the instrument (Fig. 3). Thus, signal-to-background ratio close to the elastic signal on instruments at pulsed spallation sources is usually worse than that at reactor sources. Furthermore, different experimental needs lead to the requirement of a tunable (flexible) instrument resolution, in order to trade resolution for intensity. To adjust the instrument resolution in the IN500 project, we phase one of the resolution-defining choppers to the source to cut a part of the pulse tail corresponding to the experimental requirements. By shifting in time the chopper phase, we can cut more or less of the trailing edge of the source pulse while taking full advantage of its sharp rising edge. Our calculations (Fig. 3) show that after the pulse shaping by chopper #2, the resolution function has a fairly symmetric shape, and at the same time we can achieve resolutions even better than that of IN5 at ILL and comparable to that of the backscattering spectrometer IRIS at the Rutherford-Appleton Laboratory Neutron Facility (ISIS) in England (Fig. 4). Variable secondary spectrometer resolution is achieved by the capability of selecting different slit widths on chopper #6, a counter-rotating pair of disc choppers.

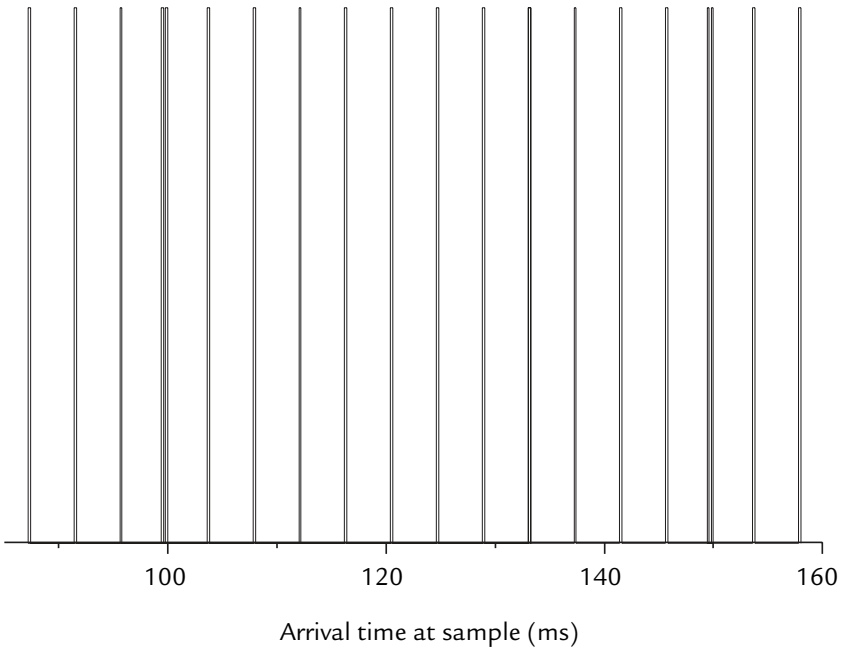

↑ ***Fig. 2.*** *Neutron pulses arriving to the sample as a function of time in twelve-fold RRM operation at the 20-Hz Lujan Center. The 240-Hz pulses between 105 and 147 ms are the useful pulses emanating from the source pulse at t = 0. Pulses around 99 and 149 ms overlap with a pulse from the previous and subsequent source pulse, respectively. The figure indicates total duration of pulses, not the true shape.*

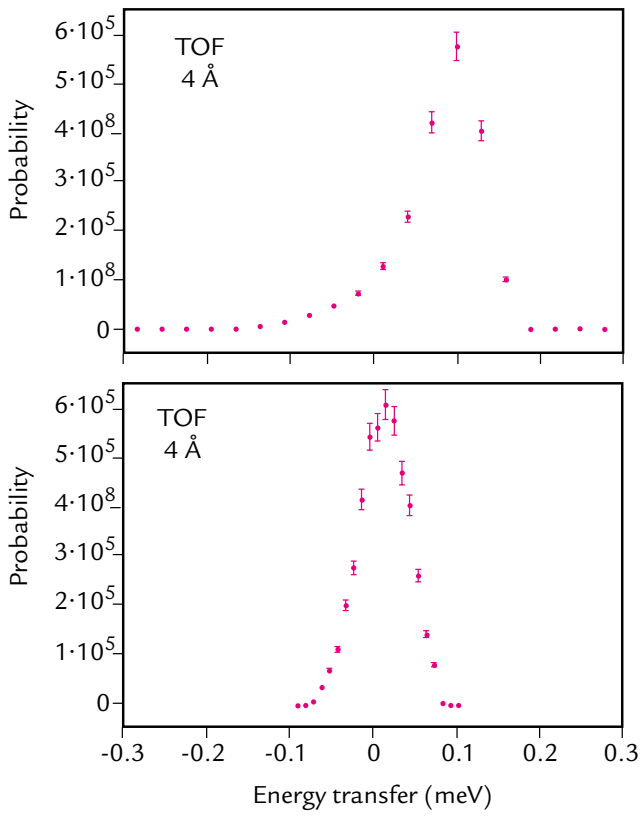

↑ ***Fig. 3.*** *Monte-Carlo simulated elastic line shapes for IN500 with no pulse tail cutting (left) and with chopper #3 phased to cut the coupled cold moderator pulse at the Lujan Center at 0.5 ms.*

Low-Losses Beam Delivery by Ballistic Neutron Guide

RRM works more efficiently the larger the distance is between the source and the sample; i.e., the smaller the difference is between the wavelengths of subsequent pulses on the sample from the same source pulse. In the case of IN500, this distance is 63 m. Intensity losses by the beam transport over such long distances are mainly caused by less than perfect reflectivity of the coatings used in the neutron guide. Thus to decrease the losses, we need to decrease the number of reflections, which can be achieved by using a ballistic guide.[1] The ballistic guide includes three parts: a nickel (Ni)-coated neutron guide with a large cross section over most of the length and diverging and converging supermirror coated sections coupling the Ni guide to the moderator and sample, respectively. The diverging guide leads to the more parallel neutron beam, which in the large cross section of the Ni-guide section leads to drastically reduced number of reflections. Based on the results of our simulation study, we expect nearly an order of magnitude better performance of the ballistic guide compared with beam transport in a conventional supermirror coated guide.[2]

Summary

The combined effect of the innovations to be implemented in the IN500—the use of a high-intensity coupled moderator; a disc chopper system capable of providing multiplied pulse repetition rates on the sample, perfect symmetric line shape, and variable resolution; and a reduced-loss neutron guide system—will

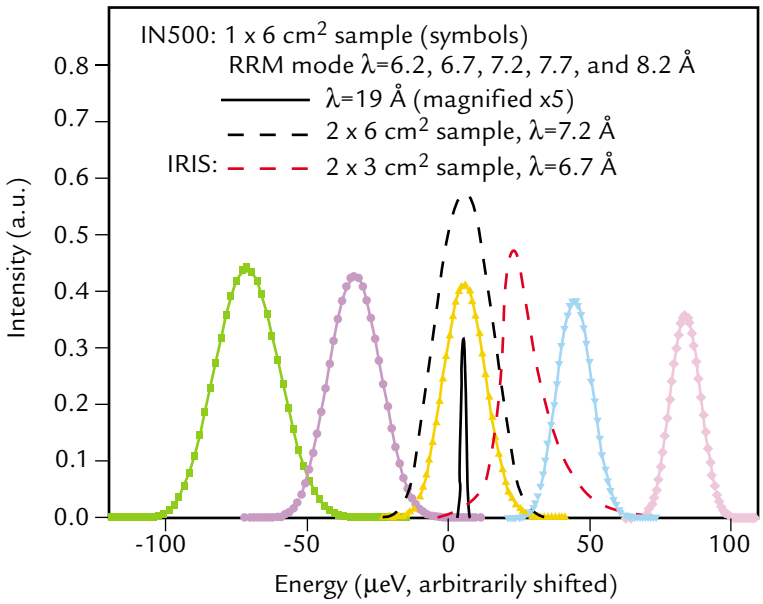

← ***Fig. 4.*** *Calculated elastic line shapes for the best resolution configuration of IN500. Chopper #3 cuts the source pulse to 220 μs FWHM length, chopper pair #6 is set to 20 μs FWHM. All pulses are centered around 0 energy, arbitrarily shifted for visibility. The symbols correspond to retaining via chopper #5 every second pulse only from a sequence illustrated in Fig. 2. The elastic response of IRIS, included for comparison, is approximately to scale in intensity.*

provide approximately 30 times more flux on the sample at the designed 160-kW power of the Lujan Center at LANL than the most powerful cold-neutron spectrometers in existence today (IN5 at ILL and NEAT at HMI). (The currently started reconstruction of IN5 is expected to bring a gain of a factor of eight to ten.) Furthermore, as test experiments at HMI have shown,[3] advanced TOF techniques make the TOF approach comparable in efficiency to the triple-axis method on the same continuous source, even for constant **q** spectroscopy in single crystals. Consequently, the IN500 project will not only deliver new capabilities in conventional applications of cold-neutron TOF spectroscopy, but it will also provide for the first time a spallation source instrument competitive with top performance cold-neutron triple-axis spectroscopy for the study of excitations in single crystals.

References

1. F. Mezei, *Journal of Neutron Research* **6**, p. 3 and references therein (1997).
2. F. Mezei, M. Russina, and S. Schorr, "The Multiwavelength Cold Neutron Time-of-Flight Spectrometer Project IN500 at LANSCE," *Physica B* **276-278** (46), 128-129 (2000).
3. F. Mezei and S. Schorr, "Time-of-Flight Constant-**q** Spectroscopy," *Physica B* **241-243** (48), 166-168 (1997).

Upgrade of the Neutron Powder Diffractometer

T.E. Proffen (LANSCE Division), T. Egami (University of Pennsylvania), S.J. Billinge (Michigan State University), A.K. Cheetham (University of California at Santa Barbara), D.A. Louca (University of Virginia), J. Parise (State University of New York at Stony Brook)

Pulsed neutron powder diffraction is a widely recognized method used in materials research to determine the structure of complex materials in a relatively short time with high accuracy. NPD is one of the most heavily used instruments at neutron-scattering centers worldwide. The Rietveld refinement method, usually used to analyze powder diffraction data, has become the standard tool for structural studies. But many crystalline materials of scientific and technological interest today, such as complex oxides, have internal disorder characterized by aperiodic local displacements of atoms. These aperiodic local deviations are better characterized by a real-space approach in which the local atomic structure is described by the atomic PDF. The PDF is the Fourier transform of the total scattering intensity, including Bragg peaks and diffuse-scattering intensities. The unique utility of PDF has been demonstrated by a number of recent studies using pulsed neutron sources to determine the local structure, and even lattice dynamics, of complex solids.[1] Understanding the real structure of complex materials can be achieved only through the combined knowledge of average and local atomic structures.

Why Upgrade the Neutron Powder Diffractometer?

Obtaining high-quality PDF data depends on two factors: (1) a large range in momentum transfer with sufficient counting statistics and (2) high resolution. The NPD at the Lujan Center is currently the instrument with the highest resolution in the United States. The instrument's resolution depends on various factors, including the scattering angle. The best resolution of $\Delta d/d \sim 0.15\%$ is achieved in the backscattering region—in other words, for large scattering angles. Currently NPD has only a relatively small number of neutron detectors at high diffraction angles (sixty-two detectors in the 148° bank). Typical data-collection times for a PDF measurement on the current NPD are up to 24 h. These long counting times make systematic exploration of the local structure of a material as a function of external parameters, such as temperature or pressure, virtually impossible. The obvious way forward is to add detectors to the instrument's backscattering region.

The NPD upgrade (Fig. 1) includes a total budget of about $1.1 M, sponsored in part by the NSF. The project involves a collaboration that includes the University of Pennsylvania, State University of New York at Stony Brook, University of Virginia, Michigan State University, University of California at Santa Barbara, and LANL. The upgrade will add 21 backscattering detector modules with a total of 168 position-sensitive ^{3}He detectors. The data-collection time is expected to be reduced by a factor of five. This addition will make the upgraded NPD a world-level high-resolution diffractometer for materials research and education. The upgrade also represents a very cost-effective approach to dramatically improving the data-collection rate. The new instrument will have the unique capability of simultaneous high-Q Rietveld analysis and PDF analysis. With the final design phase of the upgrade currently under way, we expect that the new NPD will be available to users starting with the 2003 run cycle. As such, researchers will be able to determine the average and local structures of complex materials with high accuracy and thus gain a deeper insight into the structure property relationship of modern materials. More information about total scattering and the PDF method, as well as software and references, can be found on the Total Scattering Homepage at *http://www.totalscattering.org.*

↑ ***Fig. 1.*** *Project Manager, Thomas Proffen, stands above the backscattering detectors on top of the NPD at FP1 at the Lujan Center. The shielding on top of NPD will be lifted to accommodate the new detector panels.*

References

1. T. Egami, "PDF Analysis Applied to Crystalline Materials," in *Local Structure from Diffraction*, M. Thorpe and S. J. L. Billinge, Eds., (Plenum, New York, 1998), p. 1.

DANCE—A Detector for Advanced Neutron Capture Experiments

J.L. Ullmann, R.C Haight, L.F. Hunt, E.H. Seabury (LANSCE Division), R.S. Rundberg, M. Dragowsky, M.M. Fowler, G.G. Miller, L. Pangault, J.B. Wilhelmy (C Division)

A new instrument for nuclear physics research is being built on FP14 at the Lujan Center. This state-of-the-art instrument consists of a shell of 160 barium fluoride crystals, each 15 cm long, with an inner radius of 17 cm. DANCE will be used to study the neutron-induced transmutation of radioactive elements. This process is of interest in understanding the synthesis of the chemical elements in stars, in studying the burn-up of nuclear waste, and in gaining a better understanding of archived data from past tests of nuclear explosives. Los Alamos is unique in the world in being able to make these measurements.

Why Study Neutron Capture Today?

Neutron capture is a reaction in which a neutron strikes and sticks to a target nucleus, forming a new isotope. An example of this type of transmutation reaction is the absorption of a neutron by the element ^{171}Tm to form ^{172}Tm. Usually, this new isotope is not in its ground state (the lowest energy state of a nucleus), but it rapidly decays to its ground state by emitting a cascade of gamma rays. The total energy emitted, Q, is given as $Q = M(A+1) - M(A) - M(n) + E_{neut}$, where M(A) is the mass of the nucleus with atomic number A, M(n) is the mass of the neutron, and E_{neut} is the center-of-mass energy of the neutron. The emitted gamma ray rarely has the total energy, and multiple gamma rays are usually emitted, corresponding to transitions between different nuclear levels. Typically, five or six gamma rays are emitted, each with an energy ranging from about 0.1 to 5 MeV.

The probability for neutron capture has been measured on most stable nuclei over a wide range of neutron energies. Theoretical calculations of the reaction probabilities, or cross sections, can only reproduce these measurements to within a factor of two because the process is very sensitive to details of the nuclear structure. The cross section varies with neutron energy, and for certain energies and elements, the ratio between measurement and calculation can be much greater. Currently, cross sections are needed on unstable nuclides for several problems, including understanding the synthesis of heavy elements in stars, the archived data from nuclear explosion tests, and the process behind transmuting or burning waste. Because calculations do not provide sufficient accuracy, measurements of neutron capture on these radioactive nuclei are needed, and exceedingly few measurements have been made.

The neutron energies of interest are typically from a keV to near an MeV. [Energies in nuclear reactions are measured in kilo-electron volts (keV). Stars like our Sun have energies around 1 keV.] Stellar nucleosynthesis by the slow, or s-process, which is thought to produce half of the elements heavier than iron, is believed to take place at stellar temperatures around 10 to 30 keV. The neutron energy distributions corresponding to these temperatures are shown in Fig. 1. The water moderators at the Lujan Center provide an excellent source of neutrons in this energy range.

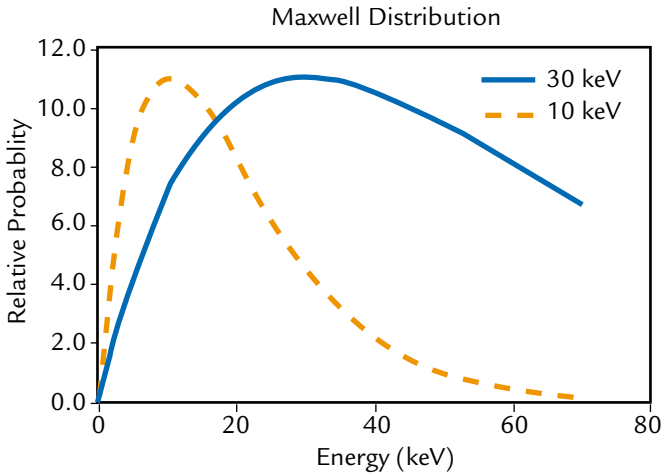

↑ ***Fig. 1.*** *The Maxwell energy distribution for neutrons at stellar temperatures of 10 and 30 keV.*

DANCE Will Use Unique Capabilities at Los Alamos

The advanced detector for neutron-capture measurements that we are building is only one of the facilities required for these important neutron-capture experiments. The intense, pulsed neutron source of the Lujan Center is required to make measurements on small quantities of target material. In fact, preliminary measurements using less efficient detectors have been made on 1-mg samples of ^{171}Tm with a 1.92-yr half-life. Even

less material will be required to make measurements on shorter half-life or less-benign radioactive targets. The radioactive material handling and fabrication facilities of C Division at Los Alamos, including the new Radioactive Species Isotope Separator, will be used to safely fabricate targets. The location of the three components necessary to make capture measurements on radioactive targets—target fabrication facilities, an intense neutron source, and an advanced detector—is unique in the world at Los Alamos.

Measuring Neutron Capture

The DANCE detector was designed to have high efficiency for gamma-ray detection, to have good neutron-energy resolution by TOF, and to be relatively insensitive to experimental backgrounds. Extensive Monte Carlo calculations were done to aid in the design process.[1]

High efficiency is needed to minimize the amount of radioactive material used for a target. For example, 1 mg of the 1.92-yr half-life nuclide ^{171}Tm produces 1.1-Ci rate of nuclear decay, and 1 Ci corresponds to 3.7×10^{10} decays per second. The need for high efficiency rules out the use of high-purity germanium detectors, which would provide excellent gamma-ray energy resolution, but at a very high cost. The alternative we chose was to use scintillating crystals coupled to photomultiplier tubes.

Background gamma rays can come both from the decay of the target and from neutron capture in detector and beam-line components induced by scattered neutrons. Target decays can produce a high background rate. A 1-Ci target, such as ^{171}Tm, produces 370 decays in 10 ns. Thin shielding and high detector thresholds could be used to reduce the backgrounds associated with low-energy gamma rays from these decays. However, to measure higher-energy gamma rays, we need a highly segmented detector made of a material with a very fast response time, such as barium fluoride.

Neutrons can be scattered into the detector from the target backing material, beam halos, and the target itself because the scattering probability often exceeds the capture probability. These scattered neutrons can be captured in the detector material, producing background gamma rays. The background from scattering can be reduced by using neutron absorbers, such as ^{6}LiH or B_4C, in front of the detector and by making the detector from materials with low-neutron-capture cross sections. Barium, for example, has one of the lowest-neutron-capture cross sections of the elements used in scintillating crystals.

With these considerations in mind, we are using a 160-segment BaF_2 crystal array designed as a calorimeter to capture all the gamma rays emitted by the target. Because the total energy, Q, is constant, a measurement of the total energy of the gamma-ray cascade provides a means of discriminating a true capture signal from the background. The segmented array also allows another way of identifying true capture events by means of cluster analysis. Gamma rays from a true capture in the target produce several clusters of hits in the array, whereas a capture in the array itself results in a single, large cluster of hits.

One way to completely cover a spherical surface is with 162 segments with four different geometric shapes. This is similar to a soccer ball, where twelve pentagons and twenty hexagonal segments are required. Two segments are left blank, for the beam to enter and exit the array. This geometry is shown schematically in Fig. 2. Fig. 3 shows the support structure for the crystal array, Fig. 4 shows a prototype of one of the four shapes of BaF_2 crystals, and Fig. 5 is a schematic representation

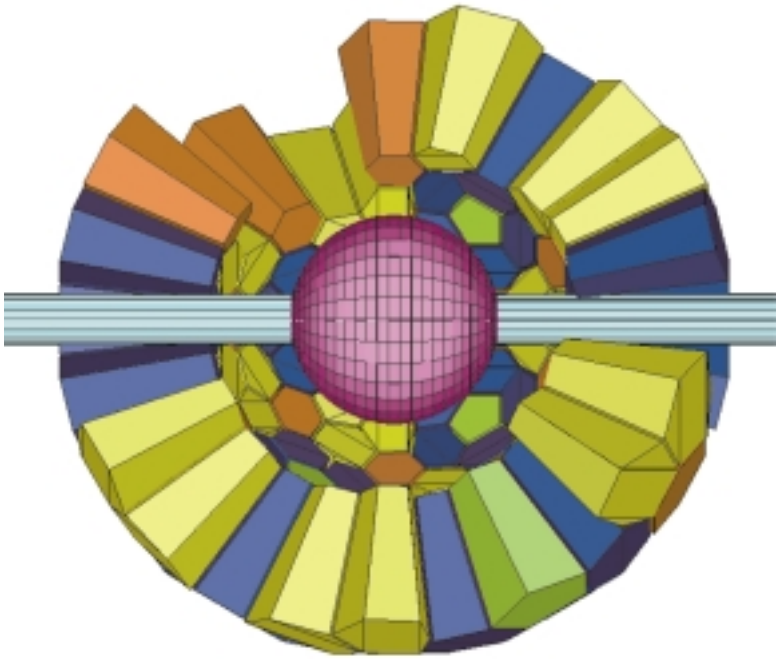

↑ ***Fig. 2.*** *Schematic representation of DANCE.*

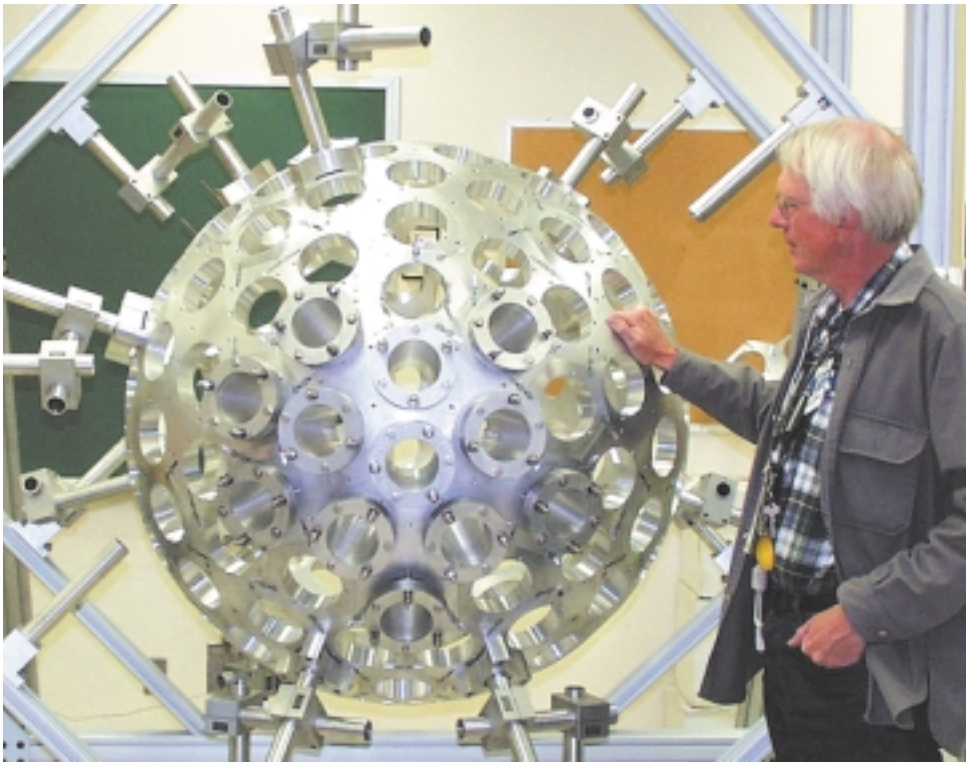

↑ ***Fig. 3.*** *John Ullmann of LANSCE-3 examines the DANCE support structure.*

↑ ***Fig. 4.*** *Prototype of one of the four crystal shapes. The crystal is 15 cm long.*

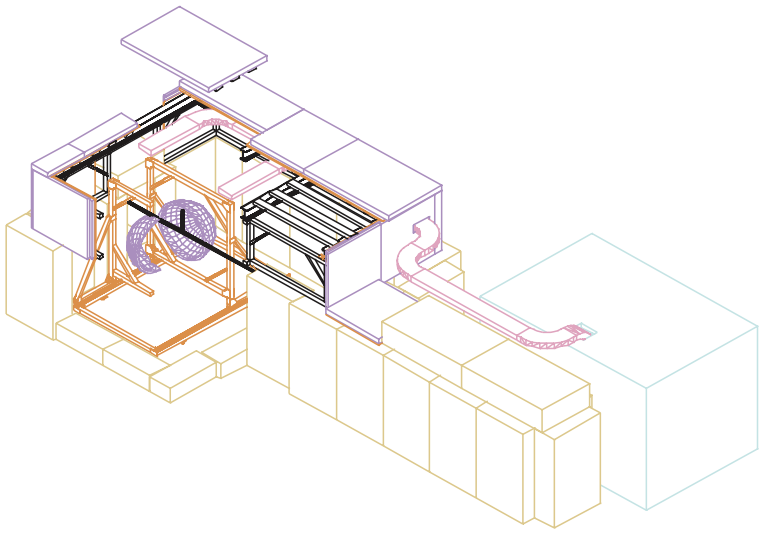

↑ ***Fig. 5.*** *DANCE experimental area.*

of the DANCE experimental area. The complete BaF_2 array will have an inner radius of 17 cm, and each crystal is 15 cm long. There is space for a 6-cm-thick shield and neutron absorber between the inner surface of the BaF_2 and the beam pipe.

Construction on FP14

The DANCE detector is being installed on FP14 at the Lujan Center. The neutron FP consists of four discrete collimators each consisting of alternating copper and 5% borated polyethylene layers with changeable inserts. Each collimator section is 81 cm long and consists of a total of 51 cm of copper and 30 cm of borated polyethylene. The last collimator ends at 19.2 m from the moderator, and the target location is designed to be at 20.5 m. The last collimator is 0.6 cm in diameter, which results in a beam spot that is uniform out to r = 0.3 cm at the target location and falls to 1/100 of the central flux by r = 0.75 cm.

The BaF_2 array is designed to be separated into two sections and can be opened to install the various targets. The radioactive targets will be sealed in evacuated 2-in.-diam beam pipes at C Division's radioactive-isotope-handling facilities so that no handling of radioactive material will be required at the Lujan Center. Various configurations of gamma shielding and neutron absorbers will be used around the target pipe as required by the individual target characteristics. The neutron beam flux will be monitored using the $^6Li(n,\alpha)$ reaction by a beam monitor downstream of the detector.

The construction of the FP is nearly complete. The mechanical support for the advanced detector has been constructed, and barium fluoride crystals are arriving from the manufacturer. The completion date depends on the production capability of the crystal manufacturer. We anticipate completion of the full array in the summer of 2002. At that time, a program of measuring several targets a year will be started. In the meantime, measurements on less demanding targets will be made with a partial array.

References

1. M. Heil, R. Reifarth, M. M. Fowler, R. C. Haight, F. Kaeppeler, R. S. Rundberg, E. H. Seabury, J. L. Ullmann, J. B. Wilhelmy, and K. Wisshak, "A 4π BaF_2 Detector for (n,γ) Cross Section Measurements at a Spallation Neutron Source," to be published in *Nuclear Instruments and Methods in Physics Research*; M. Heil *et al.*, "GEANT Simulations of Neutron Capture Experiments with a 4π BaF_2 Detector," Los Alamos National Laboratory report LA-UR-99-4046.

FIGARO—A Fast Neutron-Induced Gamma-Ray Observer

R.C. Haight, L. Zanini, M. Devlin, J.M. O'Donnell (LANSCE Division), A. Aprahamian (University of Notre Dame), J. X. Saladin (University of Pittsburgh)

Understanding nuclear reactions is key to reliable calculations of nuclear weapons, transmutation of radioactive waste from power reactors, and synthesis of the elements in stars. These calculations depend on accurate input parameters (generally more than twenty), some of which are known fairly well, but others are uncertain by uncomfortably large amounts. Progress in narrowing down the range of possible parameters depends on new types of experimental data chosen judiciously to provide the necessary understanding. We have constructed the new Fast Neutron-Induced Gamma-Ray Observer (FIGARO) FP at WNR to address many of these new types of measurements.

Pursuing Physics Research with FIGARO

Following the great successes of GEANIE—a large array of high-resolution gamma-ray detectors—FIGARO is designed for high-resolution detection of gamma rays from neutron-induced interactions with selected target nuclei (for more information on GEANIE, see *Advances in Nuclear Physics Research with GEANIE at the Weapons Neutron Research Facility* in this report, p. 106). The FIGARO layout is shown schematically in Fig. 1. Although FIGARO has fewer gamma-ray detectors than GEANIE, it offers other features including:

- extremely good collimation of the neutron beam for background reduction;
- a flexible experimental area to optimize detection efficiency and to allow for the evaluation of other detectors, such as ICEBALL (see below);
- inclusion of neutron detectors for the study of neutron-gamma coincidences (see below);
- beam time to relieve the scheduling pressure on GEANIE, which is oversubscribed; and
- a PC-based data-acquisition system.

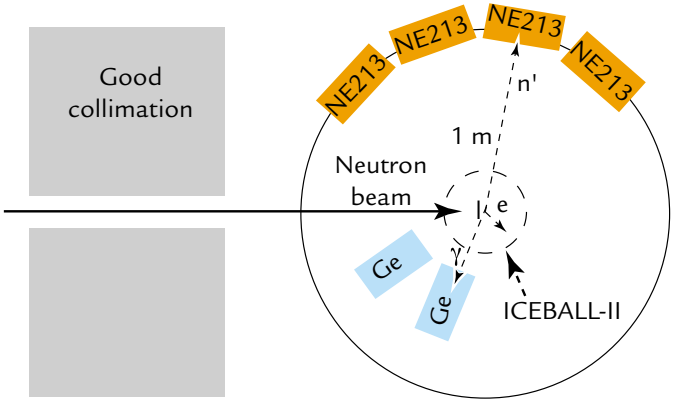

↑ ***Fig. 1.*** *Schematic layout of FIGARO showing high-resolution gamma-ray detectors, neutron detectors, and, for a different set of measurements, an internal conversion electron spectrometer array known as ICEBALL-II.*

The experimental approach with FIGARO is very similar to that of GEANIE. A pulse of neutrons, containing a wide range of neutron energies, is produced in the Target-4 spallation neutron source at WNR by the interaction of the 800-MeV proton beam from the LANSCE accelerator with a tungsten target. The neutrons, collimated to a beam of 1 to 2 cm in diameter, impinge on a sample 20 m from the source, where nuclear excitations take place. The excited nuclei decay by the emission of gamma rays, which are detected by high-resolution gamma-ray detectors near the sample. The TOF of the neutrons to the sample indicates the energy of the neutron that initiated the reaction. The gamma-ray energy indicates the particular level excited (Fig. 2). Because the neutron pulses occur 35,000 times per second, we can accumulate many events to indicate the probability (cross section) of producing particular gamma rays as a function of neutron energy (Fig. 3).

Our first measurements were on neutron interactions with ^{59}Co, where we had previously studied ^{59}Co(n,p) and ^{59}Co(n,α) reactions by detecting the emitted protons and alpha particles. Thus we already had an excellent beginning in studying at least some of the interaction possibilities. We wished to put the nuclear-reaction model calculations to more stringent tests, which can be done by measuring the gamma rays produced in the various reactions. Because we already know the quantum numbers (spins and parities) of the residual states, a comparison of the measured cross sections with calculations will tell us if angular momentum is being well handled by the calculations. For many of the gamma rays we see, the calculation does very well; an example is given in Fig. 3(a). For a few others, however, such as the example given in Fig. 3(b), the agreement is not so good. We are

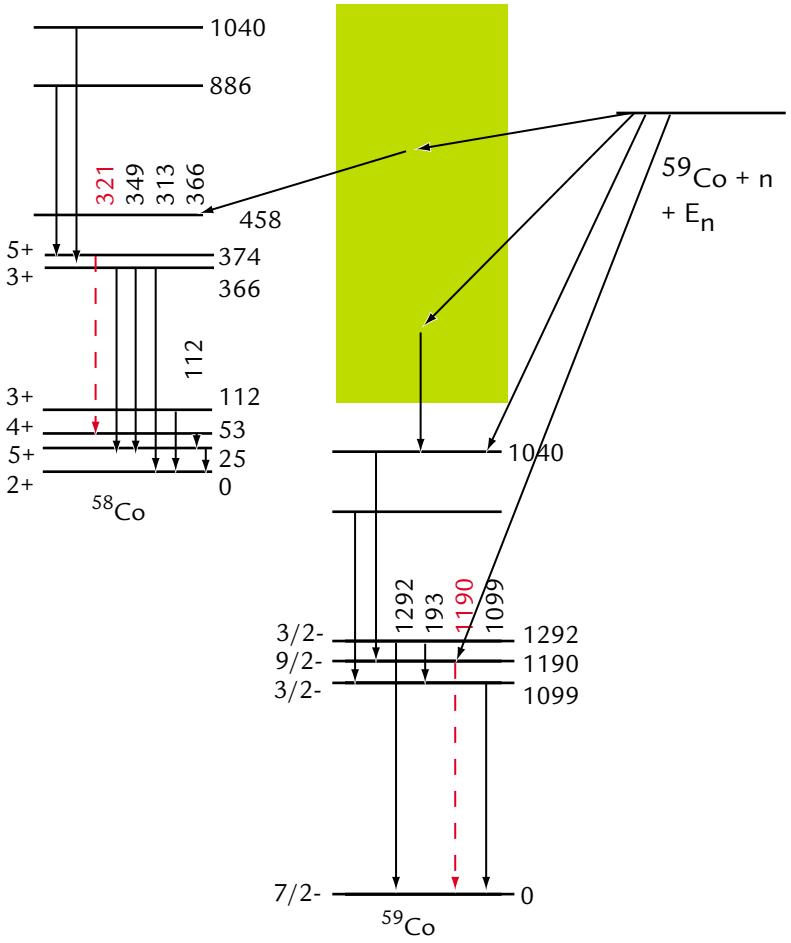

↑ ***Fig. 2.*** *An example of excitation of nuclear states by neutron-induced reactions. The initial nucleus is ^{59}Co (the only stable isotope of cobalt), which forms a compound system when a neutron of energy (E_n) interacts with it. Excited states of ^{59}Co can be created by evaporation of one neutron. States of ^{58}Co can be formed by the evaporation of two neutrons. States of other nuclei (not shown), such as ^{59}Fe, can be formed by other reactions, for example, ^{59}Co(n,p)^{59}Fe. Only a few of the many known levels of ^{58}Co and ^{59}Co are shown for simplicity. The continuous green region in ^{59}Co denotes that there are many states at these excitation energies, and most cannot be resolved.*

continuing to investigate whether the discrepant cases are due to insufficient knowledge of the levels or to some more general problem with the reaction theory.

Soon we will add neutron detection to FIGARO. The neutron detectors will be located approximately 1 m from the sample so that the TOF measurements of the emitted neutron (the " n' " in Fig. 1) can be obtained and its energy deduced. By knowing the energies of both the incident and emitted neutron energies in an (n,n') excitation, we can ascertain the excitation energy of the nucleus. We will investigate questions such as "how does the yield of a particular gamma ray then depend on this excitation energy?" Modern theories say that certain excitation energies of the nuclei emphasize certain angular momenta more than others, and the distribution of angular momenta should be reflected in the gamma-ray decay of low-lying levels, where we know the angular momenta.

Studying cobalt, where the nuclear structure and some reactions are well known, allows us to focus on more stringent tests of nuclear-reaction models. We also invoke information from nearby nuclei, such as ^{58}Ni and ^{60}Ni, where we have studied the (n,p) and (n,α) reactions. Those comparisons have led us further into studying the gamma rays from neutron-induced excitation of these nickel isotopes—measurements that were recently completed with FIGARO. Cobalt and nickel are two important structural materials in many types of nuclear-energy schemes (fission and fusion energy, for example), and so the information that we obtain has a direct connection to applications.

Yet another application of FIGARO is that of reactions on long-lived radioactive isotopes. A major goal of the AAA program is the incineration of long-lived radioactive isotopes produced as fission products in nuclear power reactors. Neutron interactions with these isotopes can transmute them into isotopes that are stable or very short-lived, so that they decay much faster. One of the major fission products is ^{99}Tc, which has a half-life of 230,000 y. We were able to obtain a sample of 50 g of this isotope and measure the gamma rays produced by neutron interactions with FIGARO. We will be comparing our results with nuclear model calculations to deduce relevant destruction cross sections, such as ^{99}Tc(n,α)^{96}Nb, ^{99}Tc(n,2n)^{98}Tc, and ^{99}Tc(n,3n)^{97}Tc.

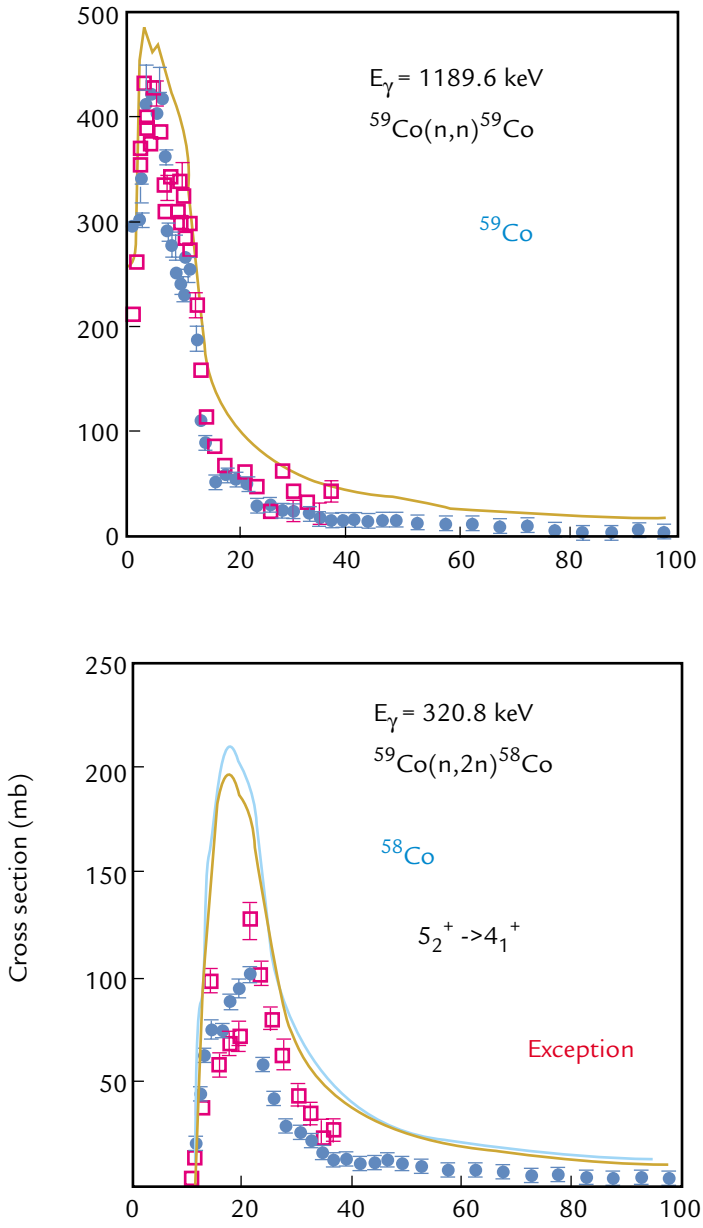

↑ *Fig. 3.* *Cross sections for creating (a) the 1189.6-keV gamma ray in ^{59}Co via inelastic scattering and (b) the 320.8-keV gamma ray in ^{58}Co from the ^{59}Co(n,2n)^{58}Co reaction as a function of incident neutron energy. The specific transitions are given in red in Fig. 2. Recent data from FIGARO are shown as the solid circles. Previous, unpublished data from ORNL[1] are shown as the open squares. The solid curves are predictions from the Los Alamos nuclear-reaction-model code GNASH.*

Commissioning of FIGARO Helped Assess ICEBALL-II Capabilities

During the commissioning phase of FIGARO, we had the opportunity to assess the capabilities of another type of detector, ICEBALL-II, from the University of Pittsburgh. This instrument detects internal conversion electrons (ICEs), which are analogous to gamma rays. With this process, instead of a transition between two levels taking place by gamma-ray emission, the energy is given to one of the atomic electrons. The probability of an ICE versus gamma-ray emission depends on the transition energy (ICE wins at lower transition energies), the angular-momentum difference (ICE wins for

larger multipolarities and for monopole transitions), and the atomic number of the nucleus (ICE does better for higher atomic numbers). We were especially interested in monopole transitions in ^{238}U, where there is no change in angular momentum and where the ICE process is the only possible mode of decay. These transitions have never been seen before in ^{238}U , and they could be relevant to GEANIE experiments that involve nuclear reactions on uranium and plutonium isotopes. We therefore excited ^{238}U with neutrons at the FIGARO beam line. Although we did not observe the ICE lines we sought, we were able to set an upper limit on the probability that these lines were produced.

In summary, we have constructed the FIGARO FP and have made initial measurements on ^{59}Co(n,*x*γ) reactions, ^{58,60}Ni(n,*x*γ) reactions, ^{99}Tc(n,*x*γ) reactions, and ^{238}U(n,conversion electron) reactions. The FP works very well, and a new PC-based data-acquisition system has provided increased reliability and utility. The addition of further detectors will allow neutron/gamma-ray coincidence measurements to put further constraints on nuclear-reaction theories.

References

1. T. E. Slusarchyk, "Preliminary Cross Sections for Gamma Rays Produced by Interaction of 1- to 40-MeV Neutrons with ^{59}Co," Oak Ridge National Laboratory report ORNL/TM-11404 (1989).

Designing Neutron Scattering and Optics Instruments with a Versatile Monte Carlo Tool Developed at LANSCE

L.L. Daemen, P.A. Seeger, R.P. Hjelm, T.G. Thelliez (LANSCE Division)

Neutron-scattering experiments require carefully designed instruments that will ensure optimal use of the beam. Unlike x-rays, neutron sources have inherently low brightness and neutrons are very expensive to produce. Designing and building an instrument to "match" the neutron source is more cost effective than modifying the source itself. The ideal scheme would be to optimize the performance of a neutron-scattering instrument and its optics to match the moderator characteristics during the instrument's design phase. We have done just that, drawing upon the experience of pioneers in the computer simulation of neutron-scattering problems, including Johnson and Stephanou,[1,2] who developed the original concept of a library of Monte Carlo subroutines for neutron optics. We have developed a public-access software program, the Neutron Instrument Simulation Package (NISP), which provides instrument designers with a general, versatile Monte Carlo tool that simulates neutron-scattering instruments while taking into account the imperfections associated with optical components.

"Cradle to Grave" Simulation Capability

NISP is a versatile and general computer simulation package that allows users to design and test a wide range of neutron scattering instruments or to simulate an experiment using computer models of instruments already created (and archived) with NISP. Users can track the history of a neutron as it journeys from the moderator to the detector. Neutron-optic models describe neutron transport and scattering as neutrons interact with the optical elements and other components on their simulated journey through an instrument. Users can monitor intermediate results such as neutron detection events in a detector, or they can visualize an instrument as a three-dimensional model (Fig. 1); manipulate a component by simply clicking on its picture; verify instrument geometry while constructing the model; and zoom in and out, change scale, rotate, translate, etc., with this unique program. NISP runs on UNIX, Linux, Windows, Mac, and DEC platforms.

The three main programs that comprise NISP are MCLIB, MC_RUN, and MC_Web. MCLIB is a library of Fortran subroutines that handles geometry representations, neutron-transport algorithms, and optical-element models. MC_RUN is a Monte Carlo engine that runs a simulation and produces a series of output files with detector counts and general information about the progress and outcome of the simulation. MC_Web is a user-friendly, Web-based application that allows the designer to set up the instrument geometry interactively without having to learn the MCLIB data structures. NISP has a tutorial to help users build their instruments or run experiments on existing models. By registering online at the Web site (http://strider.lansce.lanl.gov/NISP/Welcome.html), users will be kept informed of new features and revisions to the code via the "What's New" link on the MC_Web login page. A tutorial, a manual, and

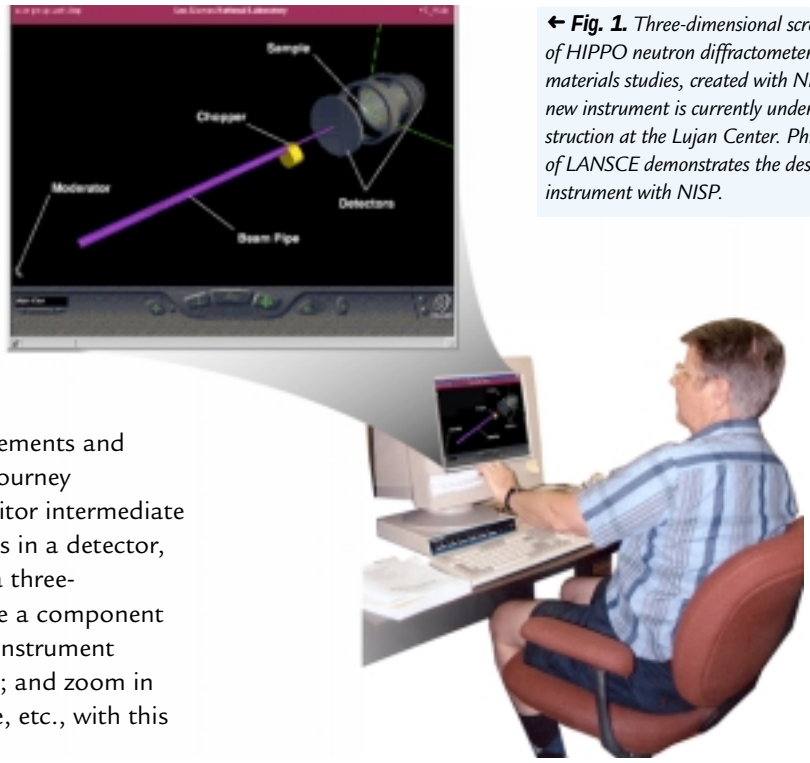

← ***Fig. 1.*** *Three-dimensional screen shot of HIPPO neutron diffractometer for materials studies, created with NISP. This new instrument is currently under construction at the Lujan Center. Phil Seeger of LANSCE demonstrates the design of an instrument with NISP.*

documentation are also available online. Users can download source code and executables free from the Web site to their computers to produce computer models of an instrument and run simulations to test its performance quantitatively, or they can run simulations of experiments on instrument models already created with NISP.

Instrument Simulation—Then and Now

The pulse emitted by a moderator at a pulsed neutron source has a complicated dependence on time, energy, and direction of emission. Because these factors impact the performance of an instrument, they must be taken into account during the design of the instrument. Moreover, many imperfections in the optical elements of an instrument can influence the instrument's performance—these effects, however, cannot be anticipated nor calculated very easily. In 1993, we began looking at the development of a tool that was needed to design an instrument suite for the LANSCE-II project. By 1994, we restructured and expanded the MCLIB code by Johnson,[1,2] and generalized existing single-purpose instrument-simulation codes to create MC_RUN.

Work began in earnest on a user interface[3] for NISP in 1995, and in 1996 the first prototype was successfully tested in time for the start of the LANSCE Enhancement Project. By 1997, we had published many applications and created a Web interface called MC_Web to allow users free access to source code and executables. In November 1997, a committee was formed to oversee the creation of an international standard for Monte Carlo libraries for instrument simulation and to develop a methodology for code maintenance and distribution. Since 1998, we have added to MCLIB a Fermi chopper, curved crystal, curved neutron guide, multi-level inelastic scattering sample, and a more general crystal model where the lattice planes are not necessarily parallel to the crystal. New elements continue to be added, and more sophisticated algorithms are being introduced for existing elements (Figs. 2 and 3). In 1999, we began working on neutron polarization and the addition of components that act on neutron spin. This new feature is important for the construction of neutron-scattering instruments geared toward the study of magnetism in matter.

This unique Monte Carlo tool automatically deals with unexpected events and takes into account the imperfections of instrument elements, such as surface roughness and chopper jitter, and complex element features, such as the time-energy distribution of the neutron pulse.

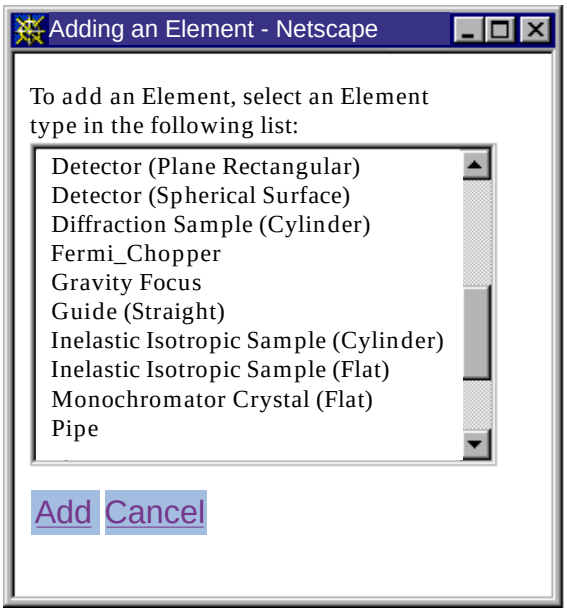

↑ Fig. 2. *Screen shot of a list of elements that can be accessed through MC_Web and incorporated in the design of an instrument. Each optical element is "pre-packaged" with an associated geometry and properties as defined in MCLIB.*

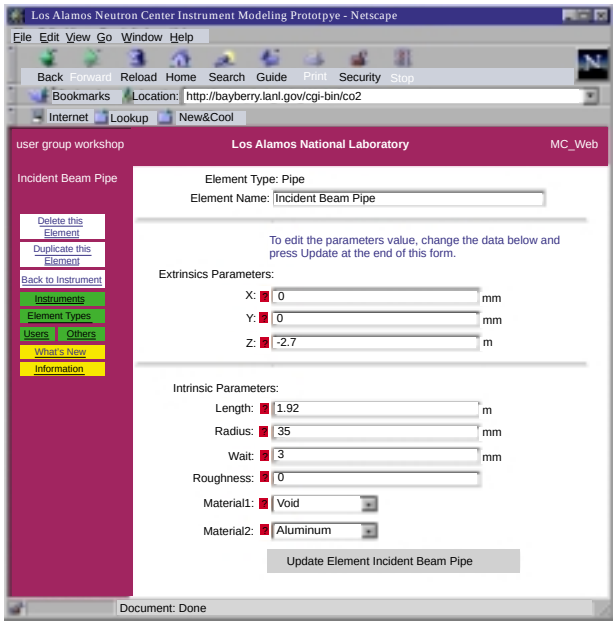

↑ Fig. 3. *Screen shot of the form used to define an element to be incorporated in an instrument. Users can add their own element types or use a large library of pre-defined elements. An online help feature assists users in defining each element and parameter.*

The program allows users to integrate simulations over a large number of instrument parameters and gain access to detailed information that is otherwise not easily obtainable experimentally, like true neutron energy in TOF methods. Idealized samples help calculate hard-to-obtain instrument characteristics, and realistic data sets provided by the program allow users to try a variety of analysis techniques. Elements or element features can be turned on and off, or can be adjusted continuously, thereby allowing the user to assess their impact on instrument performance, which is not usually possible in an actual experiment. For instance, the mosaic spread of a crystal monochromator can be set to any statistical distribution or ignored altogether—an impossible feat to accomplish with a real crystal.

Comparing Mirror Efficiency with NISP

Fig. 4 represents the configuration of a small-angle neutron-scattering instrument in the design phase, shown here as an example of the type of studies that have been performed using NISP. A mirror with the shape of a portion of an ellipsoid was incorporated into the NISP design. A useful feature of the ellipsoidal shape is that rays (in this case, neutrons) passing through one focus are reflected to pass through the other focus. We thus form an image of the collimating aperture (placed at the first focus) at the surface of the detector (placed at the second focus). When a sample is placed in the beam, neutrons are scattered at various angles, revealing long-range structure in the sample. Because the resolution of the scattering angle depends on the size of the beam spot, focusing increases count rate without spoiling resolution. MCLIB deals with all the physical interactions felt by the neutron from its emission by the moderator to its detection in the detector—transmission through the choppers, aperture, and drift spaces; reflection on the mirror surface; and small-angle scattering in the sample.

Toroidal mirrors are sometimes used to approximate an ellipsoid because they are less expensive and easier to fabricate. We used NISP to simulate an instrument with an ellipsoidal mirror so that we could compare the instrument performance with a toroidal mirror and with an ellipsoidal mirror. The results of two NISP simulations are shown in Fig. 5. The ellipsoidal mirror (Fig. 5a) behaves well—the largest apparent defocusing effect is gravity. The toroidal mirror (Fig. 5b) produces a grossly distorted image of the source. Notice that in both cases, the yellow spot at the center of the image is the answer that a simple ray-tracing approach of first-order geometric optics (ignoring aberrations) would have given.

In developing NISP, we have tried to be responsive to the needs of the neutron-scattering community. Our work can go forward only with input and feedback from the user community. We encourage users to send comments, criticisms, and requests for additional features. Much code has been written over the years to simulate very specific optical elements and neutron-scattering processes. In a number of cases, we have incorporated this legacy code in NISP to mutually benefit the author and other users of the code.

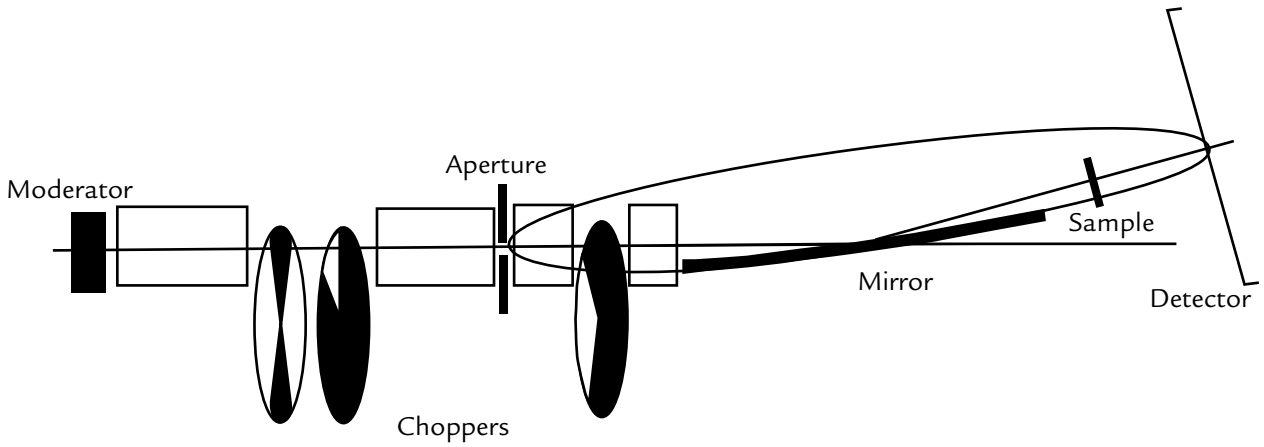

↑ ***Fig. 4.*** *A typical small-angle neutron-scattering instrument with an ellipsoidal mirror, which is used to increase neutron flux on sample. A neutron emitted by the moderator travels down the instrument axis, through the aperture, and hits the ellipsoidal mirror. The neutron is reflected, then scattered by the sample, and detected in the position-sensitive detector. The spatial distribution of neutron intensity in the detector reflects certain features of the microstructure of the sample material.*

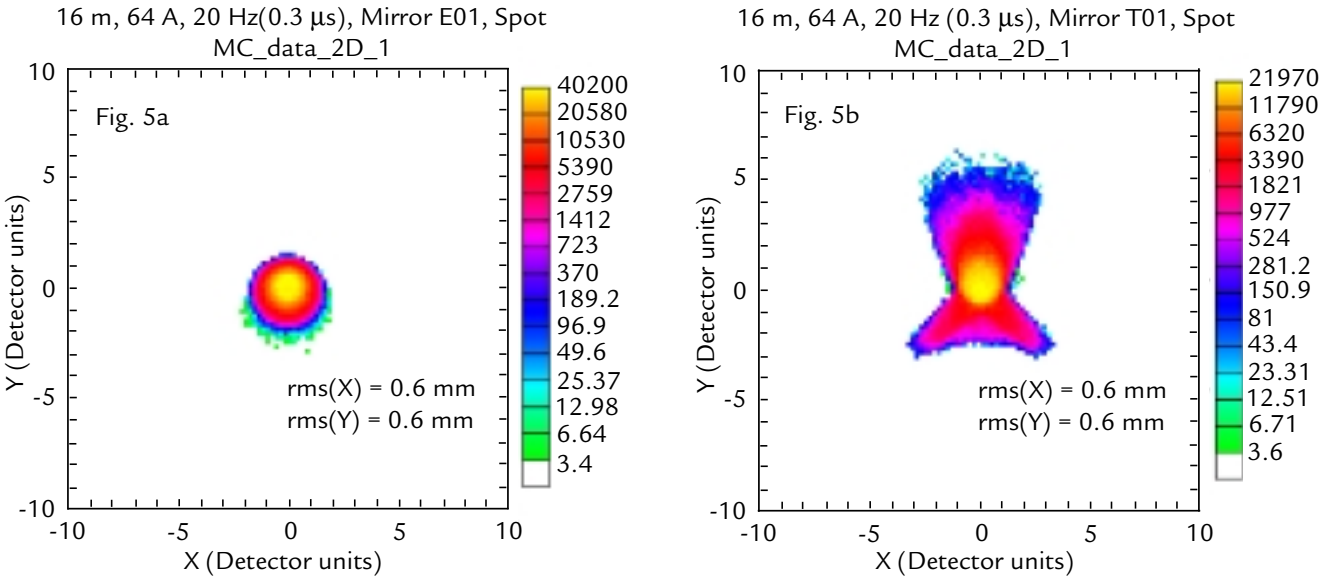

↑ ***Fig. 5.*** *A comparison between the image of a 2-mm-diam aperture produced by an ellipsoidal mirror (a) and a toroidal mirror (b).*

References

1. M.W. Johnson and C. Stephanou, "MCLIB: A Library of Monte Carlo Subroutines for Neutron Scattering Problems," Rutherford Appleton Laboratory report RL-78-090 (1978).
2. M.W. Johnson, "MCGUIDE: A Thermal Neutron Guide Simulation Program," Rutherford Appleton Laboratory report RL-80-065 (1980).
3. T.G. Thelliez, L.L. Daemen, P.A. Seeger, and R.P. Hjelm, "A User-Friendly, Graphical Interface for the Monte Carlo Neutron Optics Code MCLIB," in *Proceedings of the Thirteenth Meeting of the International Collaboration on Advanced Neutron Sources* **1**, 307-311 (1995).

Coupled Moderators at the Manuel Lujan Jr. Neutron Scattering Center

L.L. Daemen (LANSCE Division), P.D. Ferguson (Oak Ridge National Laboratory)

The Lujan Center is the first pulsed spallation neutron source to exploit the increased neutron flux provided by coupled moderators. A new partially coupled liquid-hydrogen moderator, installed as part of the LANSCE Reliability Improvement Project, delivers approximately 2.5 times the intensity produced by the previous decoupled moderator (Fig. 1a). Both the small-angle diffractometer (the LQD) and SPEAR benefit from this increased flux. Two other coupled moderators are being characterized. The first one is an ambient water moderator (Fig. 1b). It acts as a source for the PCS, which is currently in the commissioning stage. The particular coupling scheme for this moderator is expected to provide an increase in intensity by a factor of four to five compared to a decoupled water moderator. The second fully coupled moderator is a liquid-hydrogen moderator that will be put in service in 2002 (Fig. 1b).

Measuring Time Distributions

By removing all or part of the decoupling material surrounding a moderator, the reflector couples more strongly to the moderating medium (water or liquid hydrogen). This results in a very significant increase in intensity. This increase often affects the time characteristics of the pulse. Some instruments can tolerate the increase in pulse width and the appearance of a long exponential decay tail in the pulse, but others may suffer in terms of performance (resolution and bandwidth). Furthermore, the time characteristics of the pulse produced by the moderator are essential to data analysis and instrument design and optimization.

For these reasons, we measured time distributions on the partially coupled liquid-hydrogen moderator and on the coupled water moderator. The measurements were performed at several wavelengths using a small crystal analyzer spectrometer. The results were analyzed within the framework of the Ikeda-Carpenter formalism. The

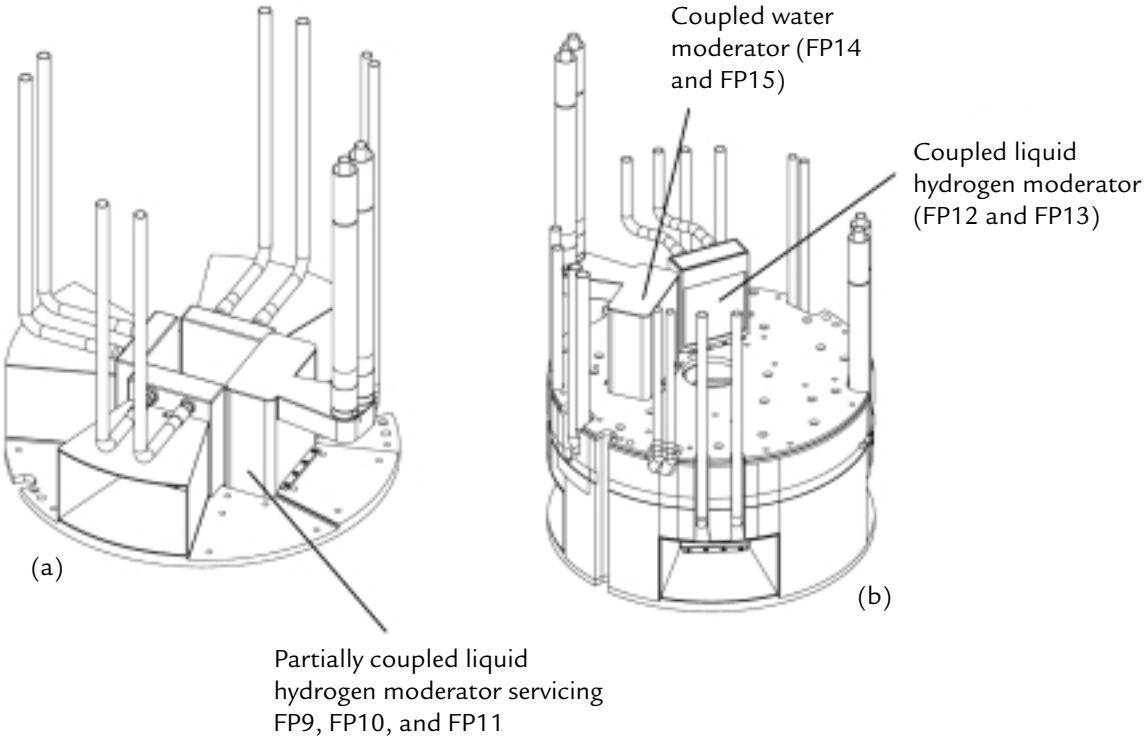

↑ ***Fig. 1.*** *Moderator configuration at the Lujan Center. Three out of six moderators are coupled or partially coupled. This results in significant increases in intensity at the cost of broader pulses with exponential tails. The liquid-hydrogen moderators are connected in series. The cryogenic fluid at 20 K produces intense bursts of long-wavelength neutrons, whereas the ambient-temperature water moderators produce shorter-wavelength neutrons. Long-wavelength neutrons tend to be more useful for the study of structures on a larger length scale.*

method enabled us to obtain detailed time-dependence information at twelve wavelengths between 1 and 20 Å in the case of the partially coupled liquid-hydrogen moderator and five wavelengths in the case of the coupled water moderator. In both cases the measurements showed shorter tails and narrower pulses than Monte Carlo calculations. Two decay constants (moderator and reflector) were clearly visible in the data.

Fig. 2 shows a typical time distribution at 6.3 Å for the partially coupled liquid-hydrogen moderator. It illustrates the quality of the fit provided by the Ikeda-Carpenter model. From such fits, it was possible to extract the main characteristics of the neutron pulse. For instance, Fig. 3 shows the FWHM of the (measured) time distributions also for the partially coupled liquid-hydrogen moderator. It is clear that coupling the moderator, even partially, leads to a significant increase in the width of the pulse at all but the shortest wavelengths. This increase tends to affect low-resolution instruments (e.g., small-angle scattering or reflectometer) less than other types of instruments, and the resulting increase in flux on sample greatly speeds up data collection.

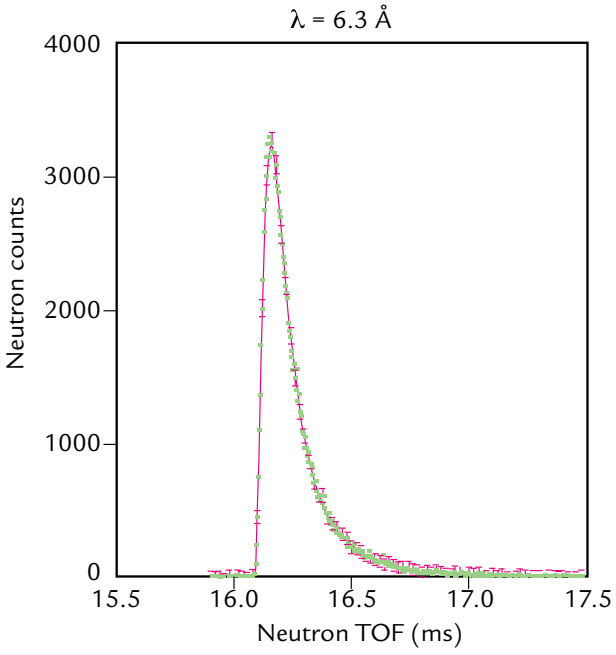

↑ ***Fig. 2.*** *Time distribution for the partially coupled moderator at 6.3 Å. The squares represent the experimental data. The solid line is a fit with the Ikeda-Carpenter formula. The asymmetric nature of the distribution (due in large part to the presence of the exponential tail at large emission times) is clearly apparent.*

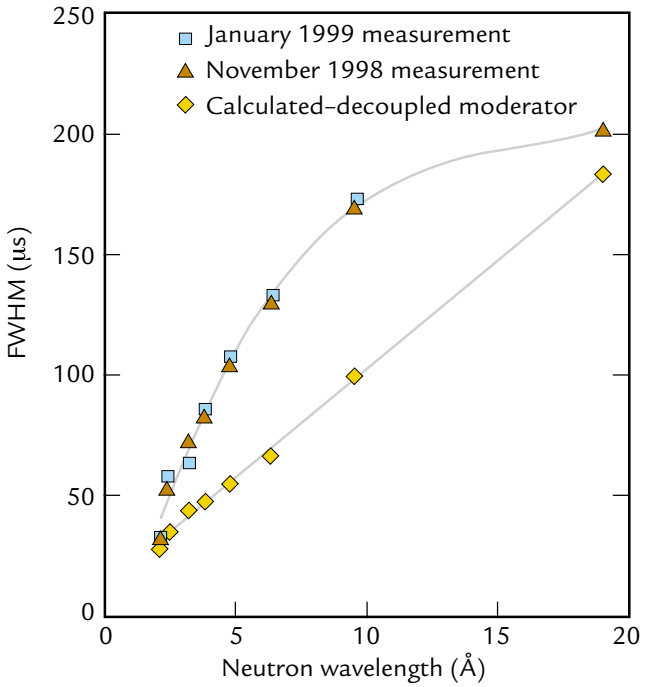

↑ ***Fig. 3.*** *Squares and triangles: FWHM of several time distributions measured on FP9 (partially coupled liquid-hydrogen moderator). Compare the results to equivalent data for a decoupled liquid hydrogen moderator (diamonds). The solid lines are guides for the eye.*

Even though much remains to be done to improve our understanding of coupled moderators, it is clear that the benefits provided for certain classes of instruments guarantee that they will become a staple of existing and future neutron sources.

Upgrades to Existing Beam-Line Safety Systems

J. Sturrock (LANSCE Division)

The Personnel Access Control System (PACS) and its extension, the Experimental Area Personnel Access Control System (EPACS), prevent exposure to prompt radiation at LANSCE by controlling access to areas in twenty locations along the primary beam line (PACS) and in the experimental areas (EPACS) where access to secondary beam lines is a concern. These two unique systems, which input to the Radiation Security System (RSS)—the umbrella radiation safety system at LANSCE—are upgrades that replace existing personnel safety systems. They comprise various innovative electronic assemblies and Kirk-key access-control hardware that are designed to achieve compliance with regulatory requirements (DOE Order 420.2 and LANL LIR 402-701-01.2), which standardize and improve the reliability and quality of access-control systems at accelerator facilities.

PACS/EPACS Description

PACS upgrades and replaces the original personnel safety system used to control primary beam-line access to prompt radiation and high-voltage hazards. EPACS upgrades and replaces the instrument-personnel-access control system used to control secondary beam-line access to prompt radiation. Being components of the RSS subjects them to the same requirements as engineered safety systems.

PACS/EPACS provides redundant contacts indicating its protective state. These are processed by the RSS to provide the required protective functions. A typical PACS system has barrier sensors that inform the system if a barrier has been opened, SCRAM switches that will stop beam delivery if pushed, sweep reset switches that verify that an area sweep has been performed, and sirens and strobe lights to warn personnel in the area of impending beam operations. A personnel interface near the area being controlled allows workers to determine whether it is safe to gain access to the affected area so that sweeps can be performed before the area is secured. The main electronics enclosure houses the relay logic that controls PACS, a programmable logic controller (PLC) that performs non-critical timing functions and communications, power supplies, and a maintenance panel that displays system conditions and faults (Fig. 1). The Kirk-key release node contains a battery backup system that ensures that the system will be able to monitor secured areas during a short power outage, and a PLC that

↑ ***Fig. 1.*** *The PACS interface panel, Kirk-key system, and yellow electronics enclosure are shown (left). An inside view of the enclosure shows the access control module and power source (right).*

monitors the beam stopper configuration to ensure that an area is safe before a key release is issued. The accelerator operator interface in the Central Control Room in conjunction with the key release node allows keys to be issued for access when the area is safe.

A typical EPACS system also has barrier sensors (modified from the PACS design to include connectors that allow the areas to be easily reconfigured), personnel interface near the area being controlled, and a battery backup and Kirk-key release node (Fig. 2). EPACS, however, automatically allows access to the controlled area when beam stoppers are inserted into the secondary beam line. EPACS has one main electronics enclosure that houses three printed circuit boards (PCBs). These PCBs are assembled with ribbon cable to allow quick field replacement. The EPACS also houses a Kirk-key release mechanism and is designed with relay logic, but the system does not have a PLC as does PACS. The reset, SCRAM, and sirens were combined into one enclosure to simplify the layout, and several new sensors were designed to accommodate fence-barrier loops.

↑ ***Fig. 2.*** *Jim Sturrock, LANSCE-6 team leader of the Protective Systems Team, pushes the reset button after completing a practice sweep of an area while demonstrating how PACS operates.*

A typical personnel sweep is controlled by a written procedure. When the sweep start button is pushed on the operator interface panel, the sirens automatically sound for 30 seconds. After the siren has sounded, the sweep team enters the area, proceeds to the first sweep station, and pushes the reset button. The team then carefully inspects the area between the first and second sweep station to be certain that no personnel are present and then pushes the reset switch on the second sweep station to verify that the area has been secured. After pushing the second reset button, the team sweeps the area between the second and third station and pushes the third reset switch to again verify that the area has been secured. This procedure continues until a sweep of the entire affected area has been completed. A timer allows the team to exit the area after the last reset switch has been pushed (Fig. 2). When the keys are returned (or the sweep is verified), the sirens are again sounded, and after a 30-s delay, the affected area is secured.

We have completed the development and installation of PACS in twenty locations along the primary beam line at LANSCE for the existing facility. The PRAD experimental facility, which is located in an existing primary beam-line area, was upgraded to PACS last year. Provisions have been made to extend PACS to new beam lines like the IPF, which is being installed at the north port in the linac transition region. A separate PACS and RSS were installed at the facility that houses LEDA, and EPACS will be installed on the four new SPSS flight paths being constructed at the Lujan Center. The system will be extended to the rest of the flight paths at the Lujan Center and to the flight paths at WNR as funding permits.

EPACS was developed by modifying PACS to account for the needs of secondary beam lines in the experimental areas in the Lujan Center, WNR, and Area A. EPACS became a natural extension of PACS into these same areas. The primary difference between the two systems is how beam-line access is allowed. In primary beam lines, access is controlled by the configuration of the accelerator beam stoppers and requires permission from accelerator operators. In a secondary

beam line, access is controlled by the beam stoppers for that particular experiment and access is allowed automatically if the area is safe (i.e., if the beam stoppers are inserted).

PACS wiring is run in dedicated conduit or cable trays because of the permanent nature of the primary beam lines. EPACS is soft wired (not in conduit) and connected by plugs to the various components that make up the EPACS system so that changes can be made to the experiment with minimal time and effort. For example, the old personnel safety system in 4FP30R at WNR is being removed to reconfigure the area with EPACS. It will take electricians several days to remove the old conduit, and if the old personnel safety system were to be reinstalled instead of EPACS, it would take them a couple of weeks to put the system back in place. The soft-wiring configuration of EPACS will allow electricians to remove the system in four hours and replace it in two days. The soft wiring and plug connections are protected by extensive interlock and fault-detection circuitry. The following general design considerations were incorporated into EPACS:

- an EPACS user-interface panel (Fig. 3) similar to PACS;
- self-checking circuitry and fail-safe design of sensor loop wiring to allow the use of soft wiring and add confidence to the integrity of the system;
- loud warning devices to warn people of impending beam-allowed conditions;
- self-directing control panels, indicating flow and status of the personnel sweep, located both at the access point and at the main enclosure to assist sweep personnel;

↑ ***Fig. 3.*** *The EPACS user-interface panel has been designed like the PACS panel so that people who access these areas will see, and become familiar with, the same interface in all areas.*

- battery backed-up Kirk-key release mechanism with provisions for a mechanical, key-controlled override for emergency access under any condition, and a key-driven restricted-access capability to allow managers to control access to an area;
- minimal power, battery backed-up indication of access control state and power source, which will allow sweep personnel to ascertain the condition of an area even in the event of loss of power; and
- battery-backed-up "secure" state to eliminate the need to re-sweep an area in the event of a power failure and yet to monitor the loop sensors to ensure that the zone remains "secure." (This final design feature saves countless man hours of accelerator operators' time to re-sweep areas after minor power glitches.)

Cooling Tower Replacement Project

During compliance sampling in 1996, National Pollutant Discharge Elimination System (NPDES) permit levels for arsenic in the LANSCE cooling tower basins were exceeded and reported to the Environmental Protection Agency (EPA). Wood slats treated with arsenic-based preservative within the cooling towers were determined to be the source of the arsenic. To address the NPDES non-compliance, we halted normal blow-down discharges. New ion exchange columns were installed at the site as an interim corrective action, and water from the cooling towers was routed through them to remove the arsenic. Operational samples were collected from cooling-tower basins. Once analytical results showed the arsenic levels in compliance with NPDES permit requirements, the ion exchange columns were removed from service and normal tower operations resumed. The Laboratory advised EPA in a letter dated February 14, 1997 (Los Alamos National Laboratory letter, ESH-18/WQ&H:97-0053) that long-term corrective actions included replacement of the cooling towers and that subject to DOE funding approval, the completion for construction of two new cooling towers was estimated to be April 1998. This schedule was revised by letter dated June 28, 2000, changing the estimated completion date for replacement of all the cooling towers to March 2002. Three independent cooling towers and cooling water distribution systems support the linear accelerator at LANSCE. Each cooling tower and its associated distribution system constitutes a complete and useable facility. Cooling tower 53-60 and its distribution system serves the injector end of the accelerator. Tower 53-62 serves the main linac portion of the accelerator (sectors B through H), which is the largest and most critical section. Cooling tower 53-64 provides cooling water to the switchyard, Area A, the PSR, WNR experimental areas, and the Lujan Center. All of these cooling towers were constructed during the initial construction of the accelerator (1969-1971).

Currently we are operating TA-53's cooling towers in two different modes. During accelerator operations when there is a large heat load on the cooling towers, blow-down is controlled by conductivity. During maintenance periods while the accelerator is shut off and heat loads are lower, cooling towers have a constant blow down or bleed rate—both terms relate to the discharge of water that can no longer be recycled through the cooling system of the accelerator. In this case, the water is discharged to an outfall to the environment and monitored closely for arsenic and chlorine levels. Our site operators are continuing to collect operations samples to monitor arsenic levels, and the ion-exchange columns are retained onsite as back-up treatment units.

Upon exceeding outfall arsenic permit limits, we developed an iterative replacement program and made commitments to EPA with the first tower to be replaced in FY1998. The second cooling tower was scheduled for completion in FY2000 and the third in FY2001. The planned approach for replacement of the towers was to construct a replacement tower and service building immediately adjacent to each of the existing towers. Although the original schedule has been delayed, our commitment to replace the towers remains the same. We have kept the New Mexico Environmental Department (NMED) abreast of the status change, and they have been supportive to date. The first of the projects—replacement of Cooling Tower 53-62—was completed in April 2001 (Fig. 1). The replacement tower is commissioned and is fully operational. This project was revised to extend the distribution system to

↑ ***Fig. 1.*** *Cooling Tower 53-62 in the foreground and replacement tower under construction in the background.*

the injector end of the accelerator, thereby eliminating the need for Cooling Tower 53-60. Tower 53-60 has been disconnected and will be torn down in FY2002. The Engineering Study and Title II Design for the replacement for Tower 53-64 were completed in FY2000. The construction contract was awarded in April 2001 with completion and tie-in scheduled for February 2002.

The new cooling tower is constructed on a concrete tower basin that matches the footprint of the new tower. To avoid the issues associated with the existing tower, the new tower is an induced draft, counter flow, multiple cell tower that was erected on site. All components are fiberglass with type 316 stainless-steel appurtenances. The ladders and guardrails are galvanized steel. Fill material is a high-efficiency cellular-fiber type formed from Polyvinyl Chloride (PVC), with two fill-pack layers maximum.

All of these projects are being managed as a successful team effort between LANSCE Facility Management, the Nuclear Weapons Program Office, and the Project Management Division.

—T. E. Belyeu (LANSCE Division)

New Radioactive Liquid Waste System Treatment Facility

LANSCE management has had long-standing concerns regarding the environmental integrity of the existing Radioactive Liquid Waste (RLW) system. RLW is generated by the particle accelerator operations and associated experimental activities at TA-53. The RLW flows through a system of underground drains to an underground tank system and is subsequently pumped for discharge to an onsite surface impoundment (lagoon). These discharges consist primarily of high-purity water that is slightly activated by contact with the accelerator beam. The existing RLW holding tanks have exceeded their useful life and may be leaking. LANL and NMED began discussions on closure of the surface impoundment in 1989 due to environmental impact concerns. LANSCE committed to NMED to end RLW discharges to the surface impoundment by the end of CY1998. The Radioactive Liquid Waste System Treatment Facility Project has replaced the existing lagoon at TA-53 with a new treatment and disposal facility. The facility includes three 30,000-gal. storage/decay tanks and two evaporative basins. The Radioactive Liquid Waste Tank Replacement Project replaced the existing holding tanks with two new double-walled lift stations.

The commitment to end discharges to the lagoon put the Radioactive Liquid Waste Tank Replacement Project on a fast-track effort with a fourteen-month design-construction schedule. Exceptional cooperation between LANSCE, the Nuclear Weapons Program Office, the Project Management Division, Facility and Waste Operations Division, and DOE demonstrated LANL's ability to complete a project ahead of schedule and under cost.

The new RLW treatment system consists of two separate but related parts. Part one replaced the existing holding tanks, and part two provided a new treatment facility and an aboveground evaporative basin, located east of the existing lagoon (Fig. 2). The old RLW tank system consisting of four existing tanks has been removed from service to prevent the potential risk of adjacent soil contamination. The tanks consist of two 2,500-gal. stainless steel tanks (with pumps) located outside Area A and two 4,500-gal. concrete tanks (with pumps) located at WNR and Lujan Center. The

↑ ***Fig. 2.*** *The evaporative basin is shown in the foreground. The RLW treatment facility is shown in the background (east to west view). The insert is a view of the 30,000-gal. storage tank in the tank vault.*

removal actions were conducted in accordance with all applicable environmental restoration requirements. It is unknown at this time if the soil around the tanks is contaminated. Any contaminated soil will be excavated and disposed of according to environmental restoration procedures. Two new lift stations have been installed, each consisting of a 2,500-gal. double-walled plastic tank set in a corrugated metal-lined hole with a concrete floor to provide defense in depth for any potential radiation spill. Each lift station is outfitted with level controls, automatic or manual controls for pumping, and associated alarm systems. Pumps provide circulation capability before sampling at installed sampling stations.

The two lift stations discharge into a gravity-flow piping system that transports RLW to the new facility, which consists of three 30,000-gal. storage tanks, a support building, associated controls and piping, and evaporative basin. A truck port is provided for transporting RLW by tanker truck and discharging any of the storage tanks. The storage tanks are housed in a below ground concrete vault as a third level of defense in depth. The storage tanks and all piping are double walled to prevent total failure.

The system manages contaminants by holding radioisotopes in the holding tanks as long as possible to allow for the maximum possible decay of short-lived isotopes before the waste is pumped to the evaporative basin. Water containing small amounts of tritium will evaporate, leaving other longer-lived isotopes to settle into sludge. The sludge will be sampled on a periodic basis and disposed of before the facility reaches 50% of the Category 3 level. The basin consists of two sections, each with a surface area of 75 ft by 75 ft lined with a non-permeable 60-mil plastic liner. The liner is contained within a concrete basin capable of containing any leak; it is coated with a non-porous material to ensure any leak is contained and collected to a sump for return to the storage system.

The facility is constructed with 100% redundancy so that maintenance can be performed while the system is operating. All pumps are duplicated, and transfer capability is provided between tanks and basins.

Davis and Associates of Santa Fe, New Mexico, constructed the facility. Management oversight for LANL was provided through a cooperative effort between LANSCE Facility Management and the Project Management Division. The RLW group that operates the RLW plant at TA-50 also operates the system. A Waste Acceptance Criteria defines acceptable levels and materials for discharge to the new system. Waste profile forms are generated for each waste stream discharging to the RLW system. Each lift station will be sampled on a periodic basis and each storage tank will be sampled prior to discharge to an evaporative basin.

An independent Readiness Assessment completed on December 17, 1999, resulted in a limited number of pre-start and post-start findings. Corrective actions associated with the pre-start findings are nearing resolution. Authorization to assume full operations was received in mid January 2000.

—T. E. Belyeu (LANSCE Division)

Cleanup of Area C

In January 1999, we became aware that we had unknowingly exploded beryllium in the containment system in Area C. In order to restart activities, we had to clean the beryllium contamination out of the containment system and surrounding area. Hazard control plans had to be modified to ensure improved protection for clean-out crews. As part of the safety

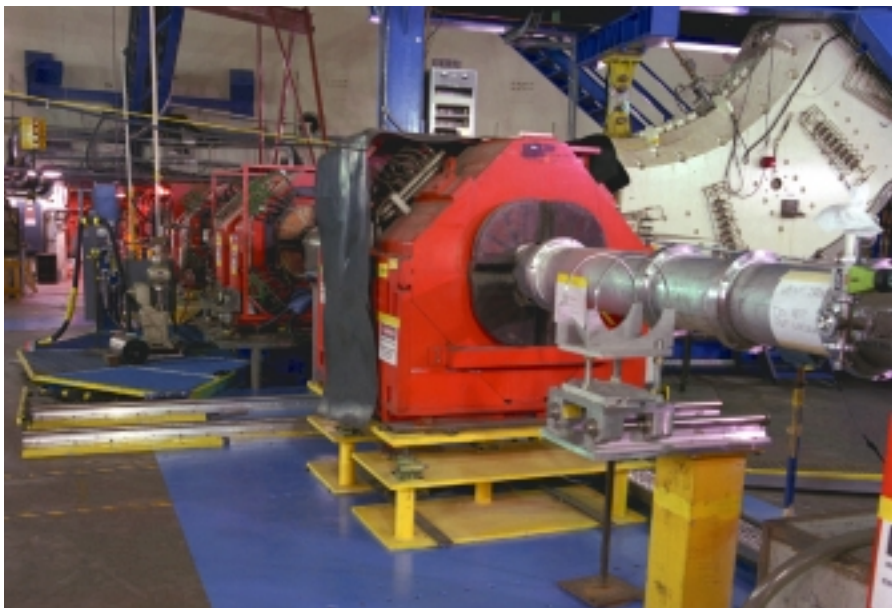

↑ ***Fig. 3.*** *View of the PRAD beam line in Area C.*

stand down, we evaluated the hazards, revisited our procedures, and engaged an independent verification panel. Hazards were addressed, and safety documentation was revised.

In conjunction with the safety stand down, we embarked on an Area C improvement project. The improvement project was a concerted effort to clean up and refurbish the area. The delay line that had been installed for APT was taken down, and uneven surfaces on the floor were milled down both for high-explosive safety and personnel safety. Extraneous equipment not pertinent to PRAD was removed, stored elsewhere, or salvaged. The Area C counting house was essentially gutted and refurbished. Aging floor panels were replaced and new carpeting was installed, countless legacy cables were removed and rerouted, current cabling was restrung, and furniture was upgraded. We accomplished all of this before we received beam at the end of May 1999.

—M. Hockaday (P Division)